Stereochemistry of hexacoordinated Zn(II), Cu(II), Ni(II) and Co(II) complexes with iminodiacetamide ligands

Natalija Pantalon Juraj,[a] Goran I. Miletić,[a] Berislav Perić,[a] Zora Popović,[b] Neven Smrečki,[b] Robert Vianello,[a] and Srećko I. Kirin[a,*]

[a] Ruđer Bošković Institute, Bijenička c. 54, HR-10000 Zagreb, Croatia

[b] Department of Chemistry, Faculty of Science, University of Zagreb, Horvatovac 102a, HR-10000 Zagreb, Croatia

Supporting Information Placeholder

ABSTRACT: Metal complexes of iminodiacetamide (**imda**) ligands and metal ions Zn(II), Cu(II), Ni(II) and Co(II) were prepared, using eight **imda** ligands (**L1**-**L8**) substituted with groups of different steric and electronic properties on the central amine nitrogen atom (hydrogen atom, methyl, isopropyl, benzyl) and the *para*-position of phenyl rings (nitro, dimethylamino). The effect of these substituents on the stoichiometry (**ML**, **ML$_2$**), geometry and stereochemistry (*mer*, *trans-fac*, *cis-fac*) of the complexes was studied in solid state, in solution and by DFT calculations. X-Ray single crystal and powder diffraction, thermogravimetry, and IR spectroscopy showed that in the solid state **imda** ligands preferentially form *trans-fac* **ML$_2$** complexes, with the exception of the *cis-fac* complex **7$_{Zn}$**. NMR spectroscopy of diamagnetic Zn(II) and paramagnetic Co(II) complexes revealed the formation of both **ML** and **ML$_2$** complexes in solution. Variable temperature NMR was used to study the effect of the substituent on the central amine nitrogen on the Zn—N bond strength and nitrogen inversion. Relative stabilities of isomers were rationalized by computations and the optimized structures used for the geometry analysis.

INTRODUCTION

Aminopolycarboxylic acids, most notably ethylene-diaminetetraacetic acid (EDTA), diethylenetriamine-pentaacetic acid (DTPA) and nitrilotriacetic acid (NTA), are some of the most widely used chelating agents. Since the first synthesis of EDTA and NTA were reported by F. Munz in the 1930s, aminopolycarboxylic acids find applications in contemporary research but also in everyday life.[1,2] For example, in the laboratory aminopolycarboxylic acids are used as metal chelators,[3–5] while Ni-NTA agarose is used for purification of proteins via affinity chromatography (His-tag method).[6] In addition, aminopolycarboxylic acids are widely used in a number of industrial processes, including paper pulp bleaching, and also as additives for household cleaning products like laundry detergents and bathroom cleansers.[1]

Iminodiacetamide (**imda**) is an aminopolycarboxylic acid derivative that can act as a tridentate *O,N,O'*-chelator, having a similar structural motif as ethylenediaminetetraacetic acid (EDTA), with amide instead of carboxylic groups. Until now, **imda** and their derivatives have been studied as chelators for PET imaging[7,8], chelators for separation of lanthanides[9] or mercury[10], ionophores for optical zinc ion-selective sensors[11], and some showed antitumor activity.[12]

Imda derivatives can serve as tridentate ligands for transition metals that form hexacoordinated complexes with **ML** and **ML$_2$** stoichiometry. Generally, for the coordination number six, two coordination polyhedra are possible: octahedron and trigonal prism.[13,14] For octahedral **ML$_2$** complexes, different geometrical isomers are known: *mer*, *trans-fac*, Δ- and Λ-*cis-fac* (see Figure S2).[15] This potential coordination variety of **imda** complexes is in opposition to hexacoordiated EDTA complexes that can only form a *cis-fac* isomer, because of the ethylene bridge linking the amine nitrogen atoms. By analyzing structures of **ML$_2$** complexes with **imda** ligands in the Cambridge Structural Database (CSD), it is apparent that they preferentially form *trans-fac* isomers. Out of the 23 known **[M(imda)$_2$]$^{2+}$** crystal structures, 22 are *trans-fac* isomers;[16,17] the only reported *cis-fac* structure is with the parent **H-imda** ligand.[18] So far metal complexes of **imda** ligands are extensively characterized in the solid state, while the characterization in solution is seldom reported.

In this work we report on the synthesis and characterization of eight **imda** ligands (**L1**-**L8**) and their Zn(II), Cu(II), Ni(II) and Co(II) metal complexes (**1$_{Zn}$**-**8$_{Zn}$**). In order to increase the solubility and enable characterization of the metal complexes in common organic solvents, terminal amides of the **imda** ligands were substituted by phenyl groups. In addition, starting from the unsubstituted ligand, electron donating or withdrawing substituents were added

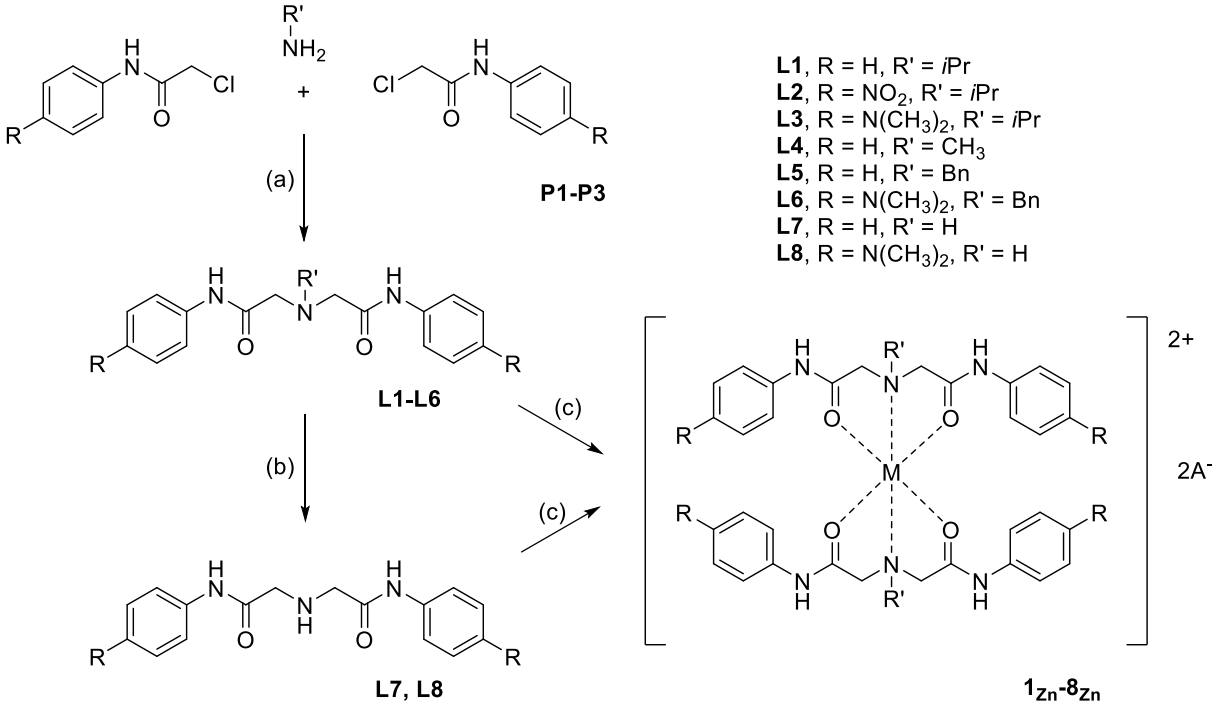

$\mathbf{1_{Zn}}$, $[Zn(\mathbf{L1})_2](BF_4)_2 \times 2CH_3OH$
$\mathbf{1_{Co}}$, $[Co(\mathbf{L1})_2](BF_4)_2 \times 2CH_3OH$
$\mathbf{1_{Ni}}$, $[Ni(\mathbf{L1})_2](BF_4)_2 \times 2CH_3OH$
$\mathbf{1_{Cu}}$, $[Cu((\mathbf{L1})_2]_2(BF_4)_2(SiF_6) \times 2H_2O$
$\mathbf{3_{Zn}}$, $[Zn(\mathbf{L3})_2](BF_4)_2$
$\mathbf{3_{Ni}}$, $[Ni(\mathbf{L3})_2](BF_4)_2$
$\mathbf{4_{Zn}}$, $[Zn(\mathbf{L4})_2](BF_4)_2$
$\mathbf{4_{nNi}}$, $[Ni(\mathbf{L4})_2](NO_3)_2$
$\mathbf{5_{Zn}}$, $[Zn(\mathbf{L5})_2](BF_4)_2$
$\mathbf{5_{nNi}}$, $[Ni(\mathbf{L5})_2](NO_3)_2$
$\mathbf{6_{Zn}}$, $[Zn(\mathbf{L6})_2](BF_4)_2$
$\mathbf{7_{Zn}}$, $[Zn(\mathbf{L7})_2](BF_4)_2$
$\mathbf{8_{Zn}}$, $[Zn(\mathbf{L8})_2](BF_4)_2$

Scheme 1. Synthesis of ligands **L1**-**L8** and complexes $\mathbf{1_{Zn}}$-$\mathbf{8_{Zn}}$. Reaction conditions: (a) DIPEA, KI, DMF, microwave 50 W, 100 °C, 1 h, open vessel; (b) H_2/Pd, 20 h; (c) ½ MA_2, M = Zn(II), Cu(II), Co(II), Ni(II), A = BF_4^-, NO_3^-, methanol.

to the **imda** system in order to evaluate their influence on the stereochemistry, stoichiometry, geometry and energetics of the studied metal complexes.

RESULTS AND DISCUSSION

Synthesis. The synthesis of ligands was carried out in several simple steps (Scheme 1). The first step was chloroacetylation[19] of aniline or its derivatives with electron donating (-$N(CH_3)_2$) or electron withdrawing (-NO_2) groups (R) at the *para*-position of phenyl rings, obtaining chloroacetamides **P1**-**P3**. The second step was nucleophilic substitution with KI as the catalyst. The addition of KI converts the chloroacetamides to more reactive iodoacetamides, accelerating the reaction.[20]

The second synthetic step was initially attempted according to a previously reported procedure,[15,16] by nucleophilic substitution in acetonitrile using potassium carbonate as a base, resulting in a mixture of mono- and disubstituted amine. Ligand **L1** was obtained in moderate yield (41%) due to low solubility of the intermediate, monosubstituted amine in acetonitrile, which precipitates from the reaction mixture and is not available for further substitution.

By changing the reaction solvent to dimethylformamide and carrying out the reaction in a microwave reactor, a higher yield of **L1** (87%) was obtained in shorter reaction time. Those conditions were successfully applied to prepare ligands **L2**-**L6**, having -Me, -*i*Pr or -Bn substituents R′ on the central amine nitrogen atom of the ligands and/or -H, -$N(CH_3)_2$ or -NO_2 groups at the *para*-position of the two **imda** phenyl rings, with yields 44-79%.

Ligands **L7** and **L8** were prepared by catalytic hydrogenation using palladium on carbon as a catalyst, to remove benzyl groups attached to the central nitrogen atom from ligands **L5** and **L6**.

Ligands **L1**-**L8** were purified by flash chromatography, and characterized by ^1H, ^{13}C NMR and IR spectroscopy as well as ESI and MALDI mass spectrometry. NMR shifts of **L1** were assigned using HSQC and COSY spectra.

Metal complexes were prepared using Zn(II), Cu(II), Co(II) and Ni(II) salts, see Scheme 1. Tetrafluoroborate (BF_4^-) or nitrate (NO_3^-) salts were used due to their weak coordinating ability, to avoid interference with the ligands being introduced into the metal coordination sphere.[15,21,22] The complexes were prepared by mixing boiling methanol solutions of the ligand and metal salt, followed by slow evaporation at room temperature ($\mathbf{1_{Zn}}$, $\mathbf{1_{Co}}$, $\mathbf{1_{Ni}}$, $\mathbf{1_{Cu}}$, $\mathbf{3_{Ni}}$, $\mathbf{4_{Zn}}$,

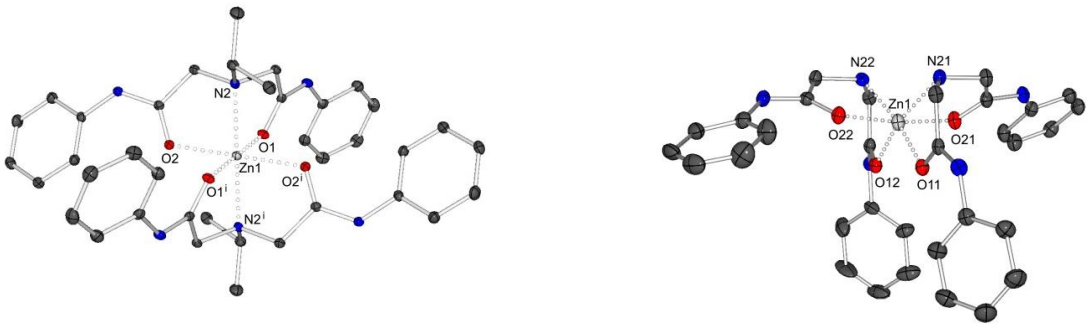

Figure 1. Crystal structures of a *trans-fac* (**1**$_{Zn}$) and *cis-fac* (**7**$_{Zn}$) isomer. (For ORTEP diagrams and crystal packing of ligand **L2** and other complexes see Figures S3-S15). Hydrogen atoms are omitted for clarity.

4n$_{Ni}$, **5n**$_{Ni}$) or vapor diffusion of hexane (**7**$_{Zn}$) or diethyl ether (**3**$_{Zn}$, **5**$_{Zn}$, **6**$_{Zn}$). The complexes were obtained in yields 43-82%, see Table S4.

Solid state characterization. Single crystal structures of ligand **L2**, three Zn(II) complexes (**1**$_{Zn}$, **6**$_{Zn}$, **7**$_{Zn}$), four Ni(II) (**1**$_{Ni}$, **3**$_{Ni}$, **4n**$_{Ni}$, **5n**$_{Ni}$), one Co(II) (**1**$_{Co}$) and one Cu(II) complex (**1**$_{Cu}$) were determined. In all determined crystal structures, **imda** acts as a tridentate ligand, forming complexes of **ML**$_2$ stoichiometry. Of the nine determined structures, eight are *trans-fac* isomers and **7**$_{Zn}$ is a *cis-fac* isomer. In Figure 1, **1**$_{Zn}$ is shown as an example of a *trans-fac* complex and **7**$_{Zn}$ as the only *cis-fac* complex.

For ligand **L2**, the solubility in common organic solvents is generally very low; therefore, we did not obtain metal complexes with **L2**. However, a single crystal structure of **L2** was determined (Figure S3). In the solid state, ligand **L2** features intramolecular hydrogen bonding forming an 8-membered ring [graph set notation S(8)], also described in literature for other **imda** ligands.[23,24] In the crystal structure of **L2**, intermolecular hydrogen bonds contribute to formation of two-dimensional layers.

Ligand **L1** was used as the representative case, having substituents of moderate steric and electronic influence, namely isopropyl at the central amine nitrogen atom (R' = *i*Pr) and unsubstituted phenyl rings (R = H). With **L1**, complexes with Zn(II), Cu(II), Ni(II) and Co(II) were studied. Complexes **1**$_{Zn}$, **1**$_{Co}$ and **1**$_{Ni}$ are isostructural slightly distorted octahedra. The ligands are bound *trans*-facially, with an angle 180° between central amine nitrogen atoms and a ≈96° (O—M—O) *fac*-angle, in good agreement with the calculated value —95.2° (see Table S10). Complexes **1**$_{Zn}$, **1**$_{Co}$ and **1**$_{Ni}$ have two methanol molecules in the crystal structure; the structure of the bulk sample was in these cases confirmed by thermogravimetry. Weight loss from 25-100 °C corresponded to loss of two methanol molecules from the crystal structure, and after heating to 1000 °C the remaining residue was ZnO, CoF_2 and NiF_2 for **1**$_{Zn}$, **1**$_{Co}$ and **1**$_{Ni}$, respectively. The similarity of IR(KBr) spectra further confirms isomorphism of **1**$_{Zn}$, **1**$_{Co}$ and **1**$_{Ni}$. Thermograms, IR spectra and powder X-ray diffractograms are shown in Supporting information.

The copper complex **1**$_{Cu}$, however, is not isostructural to other prepared complexes of **L1**. Due to Jahn-Teller distortion characteristic for Cu(II) complexes, **1**$_{Cu}$ is a distorted octahedron, with elongated apical Cu—O2 bonds (2.395, 2.400 Å). Two crystallographically independent complex cations are present in the crystal structure with differences in several characteristic torsional angles (for example in torsional angles defining the orientation of phenyl rings, see Table S2). An interesting occurrence observed in **1**$_{Cu}$, and later in **7**$_{Zn}$, is the presence of the SiF_6^{2-} anion, instead of the BF_4^- anion used in synthesis. When in solution, the tetrafluoroborate anion undergoes decomposition to fluoride ion, and the fluoride anion then reacts with SiO_2 of the glass reaction vessel forming SiF_6^{2-}.[25,26]

Trans-fac **ML**$_2$ complexes **3**$_{Ni}$, **4n**$_{Ni}$ and **5n**$_{Ni}$ were synthesized by adding methanol solutions of $Ni(NO_3)_2$ followed by $NaBF_4$ to the methanol solution of the ligand. In **3**$_{Ni}$, BF_4^- was incorporated into the crystal structure, and in **4n**$_{Ni}$ and **5n**$_{Ni}$, NO_3^- was found in the crystal structure. Phase purity of the bulk samples **3**$_{Ni}$ and **4n**$_{Ni}$ was confirmed by powder X-ray diffraction, while for **5n**$_{Ni}$, a small amount of currently unidentified phase was present.

In the crystal structure of **6**$_{Zn}$, three crystallographically independent complex cations are present. All three independent cations in **6**$_{Zn}$ have only approximate centers of symmetry located in Zn atoms. However, some structural features, like the orientation of phenyl rings [from Phe—N—$(CH_3)_2$ groups] from opposite sides of molecules differ significantly from 0°, the value expected for centrosymmetric structures (see Table S3).

Conformations of 5-membered chelate rings M–O1–C7–C8–N2 or M–O2–C10–C9–N2, denoted as E for "Envelope" and T for "Twisted" conformation are given in Table S2 for all chelate rings in all complexes. These values are obtained by calculation of the least square plane of each ring and deviations of individual atoms.[27]

Table 1. Selected bond lengths and angles for metal complexes $\mathbf{1_M}$-$\mathbf{7_M}$.

Complex	M—O1 M—O1^i (Å)	M—O2 M—O2^i (Å)	M—N2 M—N2^i (Å)	O1—M—O2 O1^i—M—O2^i (°)	N2—M—N2^i (°)
1_{Zn}	2.0951(11)	2.0944(11)	2.1822(14)	96.46(4)	180.00
1_{Co}	2.0733(11)	2.0749(11)	2.1977(14)	96.63(4)	180.00
1_{Ni}	2.0457(13)	2.0452(12)	2.1419(15)	95.85(5)	180.00
1_{Cu} (1)	2.3954(14)	1.9409(13)	2.0715(15)	96.22(5)	180.00
1_{Cu} (2)	2.4003(13)	1.9726(13)	2.0582(16)	99.87(5)	180.00
3_{Ni}	2.022(2)	2.067(2)	2.154(2)	90.02(9)	180.00
$4n_{Ni}$	2.0325(14)	2.0919(13)	2.0743(16)	87.60(6)	180.00
$5n_{Ni}$	2.079(2)	2.024(2)	2.099(3)	92.72(9)	180.00
6_{Zn} (1)	2.133(3) 2.087(3)	2.079(4) 2.112(4)	2.164(4) 2.162(4)	84.17(15) 83.11(14)	173.93(15)
6_{Zn} (2)	2.122(3) 2.127(3)	2.116(4) 2.112(4)	2.142(4) 2.136(4)	83.73(15) 83.30(14)	178.92(16)
6_{Zn} (3)	2.081(3) 2.147(3)	2.098(4) 2.098(3)	2.161(4) 2.141(4)	83.29(13) 84.97(16)	172.45(14)
7_{Zn}	2.116(4) 2.099(4)	2.097(4) 2.094(4)	2.140(5) 2.142(5)	98.10(17) 99.54(17)	103.53(19)

^{i} symmetry related atom, for $\mathbf{1_{Zn}}$-$\mathbf{5n_{Ni}}$ these are related with a crystallographic center of symmetry located in the metal atom, for $\mathbf{6_{Zn}(1)}$-$\mathbf{6_{Zn}(3)}$ these are related by an approximate center of symmetry located in the metal atom.

The only isolated *cis-fac* isomer was $\mathbf{7_{Zn}}$. The angle N–M–N of 103.53(19)° is evidence that two N atoms occupy one equatorial and one axial position of the coordination octahedron, unlike *trans-fac* isomers, where this angle is exactly 180° (for structures with crystallographic centers of symmetry) or nearly 180° (for structures with approximate centers of symmetry) (Table 1). The bond angles on the metal atom show distortion from the ideal octahedral coordination. Complex $\mathbf{7_{Zn}}$ has approximate C_2 molecular symmetry, as expected for *cis-fac* $\mathbf{ML_2}$ isomers. Although complexes of C_2 symmetry have a definite chirality, in the crystal structure of $\mathbf{7_{Zn}}$ both enantiomers are present [space group symmetry P-1, see Table S1].

Interactions governing crystal packing of the metal complexes described in this work are of ionic character because of the existence of charged cations and anions in all structures. Additionally, some of the amide hydrogen atoms form hydrogen bonds with fluorine atoms from BF_4^-/SiF_6^{2-} anions or with oxygen atoms from solvent molecules. Basic crystal packing diagrams for all structures are given in Figures S3-S15. In particular, in $\mathbf{7_{Zn}}$ additional hydrogen bonds formed by central amine hydrogen atoms H21N and H22N and fluorine atoms from the SiF_6^{2-} anion as acceptors contribute to stability of the *cis-fac* isomer in the solid state (see Figure S16). It is interesting to mention that in the only previously described *cis-fac* $\mathbf{ML_2}$ complex of **imda** ligands,[18] a similar stabilization interaction with a perchlorate counterion was found.

Characterization in solution. The stoichiometry and stereochemistry of the metal complexes were studied in solution. For diamagnetic Zn(II) complexes, ^{1}H, ^{13}C, 2D and variable temperature ^{1}H NMR spectra were recorded, either of isolated complexes or *in situ* with different ratios of ligands **L** and Zn(II) salts dissolved in deuterated acetonitrile. ^{1}H NMR spectra were also recorded for paramagnetic Co(II) complexes.

In the ^{1}H NMR (CD_3CN) spectrum of the free ligand, the α-CH_2 protons are equivalent and show a singlet (3.37 ppm for **L1**, Figure 2). When bound to the metal, the two α-CH_2 protons are no longer equivalent, showing two doublets with large geminal coupling (17 Hz for $\mathbf{[Zn(L1)_2]^{2+}}$). Two doublets indicate a *mer* or *trans-fac* isomer in solution, as opposed to four doublets (two for axial and two for equatorial α-CH_2 groups) that would be expected for a *cis-fac* isomer.[15,28]

An NMR titration of **L1** with $Zn(BF_4)_2$ was performed to study the stoichiometry of formed complexes, Figure 2. By adding Zn^{2+}, in addition to the initially present singlet of the α-CH_2 protons, two new doublets (4.02, 3.65 ppm) indicative of formation of a $\mathbf{[Zn(L1)_2]^{2+}}$ complex are present. After further addition of Zn^{2+}, two more doublets appear at lower chemical shifts (3.88, 3.49 ppm) that correspond to

the **[Zn(L1)]**$^{2+}$ complex. In an excess of Zn^{2+}, **[Zn(L1)]**$^{2+}$ is the dominant species in solution. In the NMR spectra, peaks of **L1**, **[Zn(L1)$_2$]**$^{2+}$ and **[Zn(L1)]**$^{2+}$ are separated, indicating the formation of stable complexes and a slow exchange rate between the species compared to the NMR timescale.[29]

The effect of the R' group on the Zn—N bond strength and nitrogen inversion was studied for metal complexes of ligands with different groups on the central amine nitrogen. ^{1}H NMR spectra were recorded for **ML$_2$** complexes of ligands **L1**, **L3-L8** (Figure 3). For **[Zn(L1$_2$)]**$^{2+}$ and **[Zn(L3$_2$)]**$^{2+}$, two sharp doublets were observed for the α-CH_2 protons, while one sharp singlet for **[Zn(L4$_2$)]**$^{2+}$, **[Zn(L7$_2$)]**$^{2+}$ and **[Zn(L8$_2$)]**$^{2+}$ or broad peaks for **[Zn(L5$_2$)]**$^{2+}$ and **[Zn(L6$_2$)]**$^{2+}$ were observed.

^{1}H NMR spectra were also recorded for different stoichiometry at room temperature (Figure S21). Sharp doublets of α-CH_2 protons in **ML** complexes **[Zn(L5)]**$^{2+}$, **[Zn(L6)]**$^{2+}$, **[Zn(L7)]**$^{2+}$, indicate a strong Zn—N bond, while broad signals of the corresponding **ML$_2$** complexes show a weaker bond and a Zn—N cleavage/coordination kinetics faster than the NMR timescale.[15,30] As the Zn—N bond weakens, nitrogen inversion is enabled and α-CH_2 protons are magnetically equivalent. To further study this assumption, variable temperature (VT) NMR was recorded for **ML** and **ML$_2$** complexes of **L1** and Zn^{2+}.

In VT NMR of both **[Zn(L1$_2$)]**$^{2+}$ and **[Zn(L1)]**$^{2+}$ complexes, changes of α-CH_2 peaks were observed, while all other signals remained sharp, indicating that the exchange process is limited to the α-CH_2 group (Figure 4). For the **[Zn(L1$_2$)]**$^{2+}$ complex, peak broadening of α-CH_2 was observed at 50 °C and coalescence at 70 °C, while for **[Zn(L1)]**$^{2+}$, peak broadening occurred at 70 °C and coalescence was expected to occur at significantly higher temperatures, which could not be recorded due to the boiling point of CD_3CN (80.7 °C). These results agree with the assumption that the Zn—N bond is stronger in **[Zn(L1)]**$^{2+}$ than in **[Zn(L1$_2$)]**$^{2+}$.

The exchange rate constants for these processes were determined by simulating spectra using the Mexico software

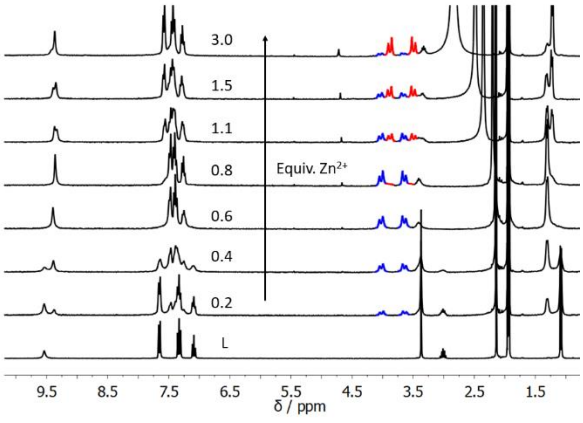

Figure 2. ^{1}H NMR (CD_3CN) titration of **L1** with $Zn(BF_4)_2$.

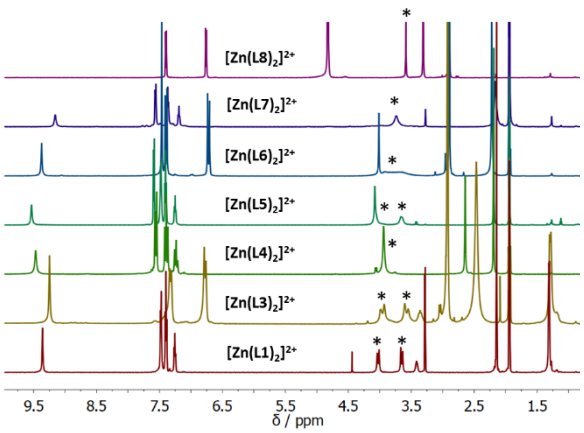

Figure 3. ^{1}H NMR (CD_3CN) of ligands **L1** and **L3-L8** and $Zn(BF_4)_2$ in a 2:1 ratio at room temperature. The α-CH_2 protons are indicated (*). **L2** was omitted due to low solubility.

as part of the SpinWorks program[31] and the energies of activation calculated using the Eyring method.[32,33] The simulated spectra and activation energy determination are shown in Figures S30-S37.

The activation energy for breaking the Zn—N bond and nitrogen inversion in **[Zn(L1)]**$^{2+}$ ($\Delta G^{\ddagger}_{298\ K}$ = 15.3 kcal mol^{-1}) was higher than for **[Zn(L1$_2$)]**$^{2+}$ ($\Delta G^{\ddagger}_{298\ K}$ = 14.9 kcal mol^{-1}), (Table S6), further supporting a stronger Zn—N bond in the **[Zn(L1)]**$^{2+}$ complex. This is not surprising, since the steric crowding of ligands in **ML$_2$** complexes lowers the strength of the N–Zn bond relative to the corresponding **ML** complexes. However, we should take into consideration that a larger temperature span would be necessary for a more accurate determination of the energy for **[Zn(L1)]**$^{2+}$.

For **[Zn(L3$_2$)]**$^{2+}$, similar temperature dependence of α-CH_2 protons is observed as for **[Zn(L1$_2$)]**$^{2+}$. Two doublets are present at room temperature, and broadening of peaks is observed at 70 °C (Figure S32).

Different temperature dependence of the α-CH_2 proton signals was observed for **ML$_2$** complexes of ligands **L4**, **L5**, **L6**, **L7** and **L8** and the results can be grouped according to the R' substituent on the amine nitrogen as follows: For R' = H (**[Zn(L7$_2$)]**$^{2+}$, **[Zn(L8$_2$)]**$^{2+}$), the α-CH_2 peak is a singlet at room temperature (Figures S28-S29), indicating a weak Zn—N bond. The ^{1}H NMR spectrum of **[Zn(L8$_2$)]**$^{2+}$ at —40 °C shows only a slight broadening of the α-CH_2 singlet indicating a somewhat stronger bond, but for observing separation of signals, spectra should be recorded at a significantly lower temperature which is not possible due to technical reasons (m.p.(CD_3CN) = —46°C). For **[Zn(L7$_2$)]**$^{2+}$, it appears that the methylene singlet broadens at 0 °C and separates into two peaks at —20 °C. At —40 °C a second species is present; the poor solubility of **[Zn(L7$_2$)]**$^{2+}$ at low temperature should also be noted.

Complex **[Zn(L4$_2$)]**$^{2+}$, R' = Me, shows a sharp singlet for α-CH_2 protons at room temperature, which slightly broadens at —20 °C; at —40 °C, two species are present (Figure S25).

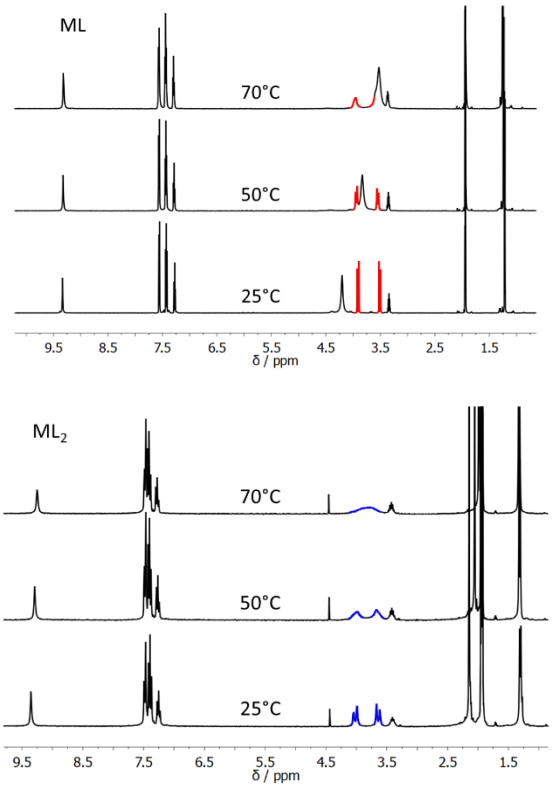

Figure 4. VT NMR spectra of $[Zn(L1)_2]^{2+}$ (bottom, stoichiometry 1:2) and $[Zn(L1)]^{2+}$ (top, stoichiometry 6:1).

Two complexes with R' = Bn, $[Zn(L5)_2]^{2+}$ and $[Zn(L6)_2]^{2+}$, show similar temperature behavior. At room temperature, the methylene signals are two separate but broad peaks. Cooling to 0 °C, the peaks sharpen into two doublets indicating a stronger Zn—N bond and by further cooling the peaks start to broaden again, due to formation of a second species (Figure S26-S27). The activation energy found experimentally for $[Zn(L5)_2]^{2+}$ is lower compared to $[Zn(L1)_2]^{2+}$ and $[Zn(L3)_2]^{2+}$ (Figure S37).

From the VT NMR studies, we found that the Zn—N bond strength is influenced by the R' substituent on the central amine nitrogen. Our results suggest that the bond strength decreases for ligands with different R' in the following order: *i*Pr > Bn > Me ≈ H, which is likely correlated with the electron-donating ability of these substituents in the same order (see also Computational Chapter).

In ^{13}C NMR of all ML_2 complexes, peaks shifted compared to the free ligand indicate complexation. Expectedly, the largest shifts were observed for groups attached to the amine nitrogen atom: 2.7 and 3.4 ppm downfield shift for CH groups of complexes of isopropyl derivatives **L1** and **L3**, 2.0 and 2.3 ppm upfield shift for CH_2 groups of benzyl derivatives **L5** and **L6**. The groups far from the donor atoms showed the smallest shifts, less than 0.5 ppm shift of the dimethylamino carbons of ligands **L3**, **L6** and **L8**.

Paramagnetic ^1H NMR spectra[34,35] were recorded for Co(II) complexes of ligands **L1**, **L3**, **L4** and **L7**. For the complex of **L1** and Co(II) at a 2:1 ratio, the spectrum shows formation of a ML_2 complex, with a small amount of signals of the free ligand (Figure 5). At a higher ratio of Co(II), 4:1, a mixture of the ML_2 and **ML** complex can be observed, which, as in the NMR of Zn(II) complexes, shows that an excess of metal ions is necessary for formation of the **ML** complex. The same was observed for **L3**, however, Co(II) complexes of **L4** and **L7** (Figures S39-S42) showed only the **ML** species at a 4:1 ratio, indicating that the equilibrium is shifted to the **ML** already at lower ratios of Co(II), possibly due to the weaker N–M bond in complexes of ligands **L4** and **L7** .

Computational Analysis. Relative stabilities of *mer*, *trans-fac* and *cis-fac* isomers of the hexacoordinated $[Zn(L)_2]^{2+}$ complex cations with ligands **L1**-**L8** were calculated in acetonitrile solution. Moreover, complex cations of several model ligands **L9**-**L14** were included (Figure 6), providing additional structural and electronic information about the studied systems. The aim was to gain insight into various effects contributing to the stereochemical preference of the **ML2** complexes, namely the effect of (i) the central *N*-substituent, (ii) the presence of the amide *N*-phenyl moiety, and (iii) the substitution pattern within the latter aromatic fragment.

Fourteen cations were studied using DFT M05-2X methodology, in line with our previous work on metal complexes of the bis(2-picolyl)amine ligand.[15] In particular, $[ZnL_2]^{2+}$ complexes with **L1**–**L9** ligands were calculated, having either unsubstituted or monosubstituted phenyl rings, as well as with **L10**–**L12**, with 3,5-disubstituted or pentasubstituted phenyl moieties. In addition, complexes **L13**–**L14** with unsubstituted terminal amides were also considered, see Table 2.

For the parent ligand **L7**, with unsubstituted central amine nitrogen and amide *N*-phenyl fragment, the stability of all three isomers is spanning a narrow range of only 1.1 kcal mol^{-1}, being the smallest range among all other systems studied here. Calculations predict the *cis-fac* isomer

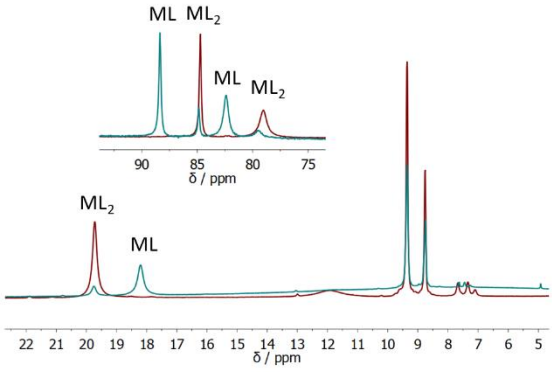

Figure 5. Paramagnetic ^1H NMR (CD_3CN) of ligand **L1** and $Co(BF_4)_2$ in ratios 2:1 (red) and 1:4 (blue).

Table 2. Calculated relative stabilities of imda (R'/R) isomers (ΔG_{TOTAL} / kcal mol^{-1}). Boldface numbers indicate thermodynamically most stable structures.

Complex	Substituents	mer	trans-fac	cis-fac
$[Zn(L1)_2]^{2+}$	*i*Pr/H	0.5	**0.0**	1.9
$[Zn(L2)_2]^{2+}$	*i*Pr/NO_2	2.6	**0.0**	0.5
$[Zn(L3)_2]^{2+}$	*i*Pr/NMe_2	**0.0**	0.7	3.7
$[Zn(L4)_2]^{2+}$	Me/H	**0.0**	5.0	3.8
$[Zn(L5)_2]^{2+}$	Bn/H	**0.0**	4.6	2.8
$[Zn(L6)_2]^{2+}$	Bn/NMe_2	**0.0**	3.7	3.3
$[Zn(L7)_2]^{2+}$	H/H	0.8	1.1	**0.0**
$[Zn(L8)_2]^{2+}$	H/NMe_2	0.3	1.6	**0.0**
$[Zn(L9)_2]^{2+}$	*t*Bu/H	2.0	**0.0**	1.3
$[Zn(L10)_2]^{2+}$	*i*Pr/$(NO_2)_2$	1.4	**0.0**	0.5
$[Zn(L11)_2]^{2+}$	*i*Pr/$(NMe_2)_2$	5.4	**0.0**	1.1
$[Zn(L12)_2]^{2+}$	*i*Pr/$(CN)_5$	7.2	2.1	**0.0**
$[Zn(L13)_2]^{2+}$	*i*Pr/amide	1.2	**0.0**	0.5
$[Zn(L14)_2]^{2+}$	Me/amide	**0.0**	5.2	2.8

of **[Zn(L7)$_2$]$^{2+}$** as the preferred structure, being 0.8 and 1.1 kcal mol^{-1} more stable than the analogous *mer* and *trans-fac* isomers, respectively. The experimentally determined X-ray single crystal structure of **7$_{Zn}$** was also a *cis-fac* isomer, although additionally stabilized by hydrogen bonding to the SiF_6^{2-} anion.

Interestingly, substitution of the central amine nitrogen reverts the stability trend among isomers in favor of some other stereochemistry. Substitution of the amine hydrogen with the methyl group, as in **L4**, promotes *mer* as the most stable isomer, being much more stable than both *cis-fac* (3.8 kcal mol^{-1}) and *trans-fac* (5.0 kcal mol^{-1}). This trend, although with slightly smaller differences, is maintained in the benzyl derivative **L5** as well. Yet, attaching a stronger electron-donor, the isopropyl group as in **L1**, overcomes the stability of *mer*, making the *trans-fac* isomer 0.5 kcal mol^{-1} more stable. This trend is further confirmed in the *tert*-butyl derivative (**L9**), where *trans-fac* is as much as 2.0 kcal mol^{-1} more stable than *mer* (and 1.3 kcal mol^{-1} than *cis-fac*), indicating that stronger electron-donating N-alkyls promote stability of the *trans-fac* stereoisomer. The latter is supported by the corresponding Hammett substituent σ_p constants being –0.09, –0.15 and –0.20 for Bn, *i*Pr and *t*Bu groups, respectively.[36]

In addition, a lower stability of *cis-fac* isomers in *N*-substituted **L1**, **L4** and **L5** can also be looked at through the steric crowding around the amine nitrogen, where the introduced substituents start to interfere with the coordination around the zinc cation and work towards favoring arrangements other than *cis-fac*. For example, in the *cis-fac* of **[Zn(L7)$_2$]$^{2+}$**, both amino hydrogens are 4.189 Å apart from each other, and come only within 3.35–3.40 Å from the nearest methylene –CH_2– hydrogens from the neighboring **L7** ligand. On the other hand, the substitution of these amino hydrogens with the *N*-methyl group, moves methyl hydrogens to the closest distance of 3.75 Å from each other, and within 2.59 Å from the matching methylene H-atoms, which clearly destabilizes the *cis-fac* isomer of **[Zn(L4)$_2$]$^{2+}$**. Such steric hindrance is relieved in the *mer* isomer, making it 3.8 kcal mol^{-1} more stable than the analogous *cis-fac*.

Although distant from the coordinating amide carbonyl fragments, substitution within the amide *N*-phenyl moiety exerts notable influence on the stereochemical preference, with a consistent observation that electron-donating groups work toward the stability of *mer*, while electron-withdrawing substituents promote the stability of *trans-fac* isomers. This is evident in, for example, the fact that electron-withdrawing *p*-nitro groups increase the stability of *trans-fac* over *mer*, from 0.5 kcal mol^{-1} in **L1** to 2.6 kcal mol^{-1} in **L2**. On the other hand, electron-donating *p*-dimethylamino groups overcome the lower stability of *mer* in **L1**, making it 0.7 kcal mol^{-1} more stable than *trans-fac* in **L3**. Even in **L8**, the attached *p*-NMe_2 group increases the stability of its *mer* analogue, yet not enough to make it more stable than *cis-fac*. Still, the relative difference between *mer* and *trans-fac* is reduced from 0.8 kcal mol^{-1} in **L7** to 0.3 kcal mol^{-1} in **L8**.

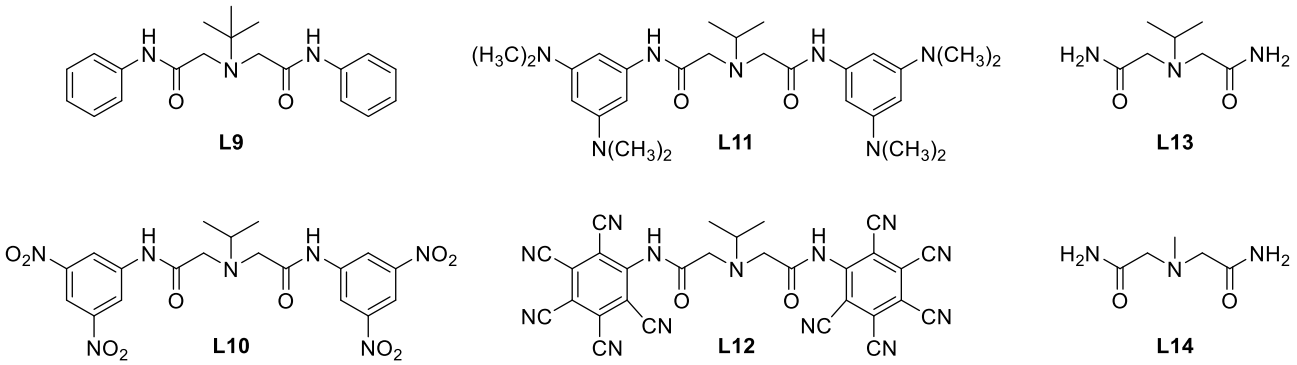

Figure 6. Ligands **L9**-**L14** used in calculations.

Unfortunately, the revealed trend is not maintained in doubly- or penta-substituted ligands **L10–L12**, where steric crowding starts to predominate over electronic influence, and where consistent structure-stereochemistry relations become less evident. For example, regardless of their electronic character, both dinitro- and didimethylamino substituents in **L10** and **L11**, promote the stability of the corresponding *trans-fac* isomers. Interestingly, the pentacyano substitution in **L12** strongly promotes the stability of *cis-fac*, being 7.2 and 2.1 kcal mol^{-1} more stable than its *mer* and *trans-fac* analogues.

Lastly, by analyzing the results for the unsubstituted amide ligands **L13–L14**, one concludes that the amide *N*-phenyl group has only modest effect on the preferred stereochemistry. Removal of aromatic fragments in **L1** and **L4** leaves the stereochemical preference intact, while their presence allows the option to fine-tune the stereochemistry through its substitution.

Structures of complexes $[\mathbf{Zn(L1)_2}]^{2+}$ and $[\mathbf{Zn(L7)_2}]^{2+}$ calculated by DFT and obtained by X-ray diffraction were used to compare the geometry of different isomers (*mer*, *trans-fac*, *cis-fac*). The geometry was analyzed by three classification methods[37–40] (see Experimental), and the results are shown in Tables S7 and S8. All three classification methods show that the complexes are somewhat distorted octahedra. Both for $[\mathbf{Zn(L1)_2}]^{2+}$ and $[\mathbf{Zn(L7)_2}]^{2+}$, the calculated structures are more distorted than the experimental structures, as a consequence of different conformations of the 5-membered chelate rings.

CONCLUSIONS

Eight iminodiacetamide (**imda**) ligands **L1-L8** were synthesized by microwave assisted nucleophilic substitution of primary amines with chloroacetamide precursors. The **imda** ligands were used in the preparation of metal complexes with divalent cations Zn, Cu, Ni and Co. Single crystal structures were determined for one ligand (**L2**) and nine metal complexes. The solid state structures of metal complexes of $\mathbf{ML_2}$ stoichiometry show *trans-fac* stereochemistry, with the exception of a *cis-fac* isomer found for $\mathbf{7_{Zn}}$ (R, R' = H).

NMR spectroscopy in acetonitrile was used to study selected Zn(II) and Co(II) complexes with various stoichiometry. When comparing **ML** and $\mathbf{ML_2}$ complexes, a stronger Zn—N bond was observed in the **ML** complexes. Based on the α-CH_2 peak shape, the strength of the neighboring Zn—N bond was found to decrease for ligands with different substituents on the central nitrogen atom, in the order: *i*Pr > Bn > Me ≈ H.

DFT calculations for three isomers (*mer*, *trans-fac*, *cis-fac*) of fourteen Zn(II) complex cations with **imda** ligands employing the implicit SMD acetonitrile solvation were applied to support experimental results. The analysis of both experimental and calculated structures using three different methods showed distorted octahedral geometries. The results show that the parent unsubstituted ligand **L7** forms a *cis-fac* isomer and upon substitution on the central nitrogen atom, other orientations prevail, *mer* with Me and Bn, while *trans-fac* with a stronger-electron donating *i*Pr and *t*Bu. In addition, computations revealed that the presence of the *N*-phenyl group does not have a significant impact of the stereochemistry, while allowing options to fine-tune the desired stereochemistry through the substitution, with an important conclusion that electron-donating groups favor *mer*, while electron-withdrawing substituents promote *trans-fac* orientations.

In this publication we show that the stereochemical preferences of $[\mathbf{M(imda)_2}]^{2+}$ complexes can be greatly influenced by substituent effects. Lessons learned herein can serve as useful guidelines for future design of organic ligands if a preferred stereochemistry of their metal complexes is desired. Recently, we are interested in metal complexes with chiral intramolecular non-covalent interactions, including selective catalysts and anticancer agents.[41-44] Stabilizing the *cis-fac* $[\mathbf{M(imda)_2}]^{2+}$ isomer by similar interactions would allow a number of interesting applications. Research along these lines is in progress in our laboratories.

EXPERIMENTAL

General remarks. Reactions were carried out in ordinary glassware and chemicals were used as purchased from commercial suppliers without further purification. Reactions were carried out in a microwave reactor (CEM Discover). Reactions were monitored by TLC on Silica Gel 60 F_{254} plates and detected with UV lamp (254 nm); ligands were purified using automated flash chromatography (Teledyne Isco CombiFlash Rf) equipped with a UV detector (254 nm) and pre-packed silica columns. Mass spectra were recorded on a HPLC-MS system (Agilent Technologies 1200) coupled with a 6410 Triple-Quadrupole mass spectrometer, operating in a positive ESI mode. NMR spectra were obtained on a Bruker Avance 300 or 600 spectrometer, operating at 300 or 600 MHz for ^{1}H and 75 or 150 MHz for ^{13}C. If not mentioned otherwise, the spectra are recorded at room temperature. Chemical shifts, δ (ppm), indicate a downfield shift from the residual solvent signal (1.94 ppm CD_3CN for ^{1}H NMR, 118.26 ppm CD_3CN or 49.00 ppm CD_3OD for ^{13}C NMR). Coupling constants, *J*, are given in Hz. The paramagnetic ^{1}H spectra of Co^{2+} complexes were acquired with a 51020 Hz spectral window, pulse width of 30°, and acquisition time of 0.16 s with no relaxation delay.[41,42] An exponential line broadening of 2 Hz was applied prior to Fourier transformation. Infrared spectra were recorded using KBr pellets with a Bruker Alpha FT-IR spectrometer, in the 4000–350 cm^{-1} region. The powder diffractograms were measured on a PANalytical Aeris instrument; conditions: Bragg-Brentano geometry (θ-2θ), source Cu-Kα (λ=1.5418 Å), measurement from 5° to 70° (2θ), with 5.2°/min (0.0216° step and 0.25 s/step). The high-resolution mass spectra were obtained with a MALDI TOF/TOF instrument with α-cyano-4-hydroxycinnamic acid (CHCA) as the matrix. Complexes $\mathbf{1_{Cu}}$, $\mathbf{3_{Zn}}$, $\mathbf{3_{Ni}}$, $\mathbf{4_{Zn}}$, $\mathbf{5_{Zn}}$, $\mathbf{5n_{Ni}}$, $\mathbf{6_{Zn}}$, $\mathbf{7_{Zn}}$,

$\mathbf{8_{Zn}}$ were desalted using Thermo Scientific Aspire RP30 Desalting Tips. For complexes $\mathbf{1_{Cu}}$ and $\mathbf{7_{Zn}}$, the molecular ion could not be observed, due to the difficulty of working with SiF_6^{2-} salts.

Synthesis of chloroacetamide precursors **P1-P3** is described in Supporting information.

Synthesis of ligands L1-L8, general procedure. A mixture of the amine (1 eq), chloroacetamide (2.5 eq), N, N-diisopropylethylamine (DIPEA) (4 eq) and KI (1 eq) in DMF (4 mL) was heated in a microwave reactor for 1 h (50 W, 100 °C). The product was extracted into ethyl acetate and washed 3 times with saturated $NaHCO_3$ and brine, the organic layer dried over anhydrous sodium sulfate, filtered and evaporated in a vacuum. The crude ligand was purified by automated flash chromatography on a pre-packed silica gel column (12 g).

(Ph-imda)-*i*Pr, **L1**. Isopropylamine (100.4 µL, 1.2 mmol), **PhNH-COCH$_2$Cl, P1** (500.0 mg, 2.9 mmol), DIPEA (815.9 µL, 4.7 mmol), KI (195.7 mg, 1.2 mmol). Automated flash chromatography 0% → 5% methanol in dichloromethane, R_f = 0.36, 5% methanol in dichloromethane. Yield: 335.2 mg (1.03 mmol, 87%), white powder. ^{1}H NMR (300 MHz, CD_3CN) δ/ppm: 9.53 (s, 2H, H_N), 7.65 (d, 4H, H_o, J = 7.8 Hz), 7.33 (t, 4H, H_m , J = 7.9 Hz), 7.09 (t, 2H, H_p, J = 7.4 Hz), 3.37 (s, 4H, H_α), 3.00 (m, 1H, H_1), 1.08 (d, 6H, H_2, J = 6.6 Hz). ^{13}C NMR (150 MHz, CD_3CN) δ/ppm: 171.9 (C_β), 139.8 (C_i), 129.8 (C_m), 124.6 (C_p), 120.4 (C_o), 56.8 (C_α), 54.1 (C_1), 18.9 (C_2). ESI-MS (m/z): 348.1 (M+Na$^+$, 14%), 326.1 (M+H$^+$, 97%). MALDI-HRMS (m/z): calcd 326.1863 ($C_{19}H_{23}N_3O_2$ + H$^+$), found 326.1863. IR (KBr) $\tilde{\nu}$/cm^{-1}: 3442, 3199, 3132, 2965, 1686, 1654, 1600, 1552, 1499, 1313, 1248, 941, 752, 691, 503.

(*p*-O$_2$N-Ph-imda)-*i*Pr, **L2**. Isopropylamine (79.4 µL, 0.9 mmol), ***p*-O$_2$N-PhNH-COCH$_2$Cl, P2** (500.0 mg, 2.3 mmol), DIPEA (644.9 µL, 3.7 mmol), KI (154.7 mg, 0.9 mmol). Automated flash chromatography 0% → 5% methanol in dichloromethane, R_f = 0.26, 3% methanol in dichloromethane. Yield: 240.3 mg (0.58 mmol, 62%), yellow powder. ^{1}H NMR (300 MHz, CD_3CN) δ/ppm: 10.03 (s, 2H, H_N), 8.24-8.17 (m, 4H, H_m), 7.94-7.85 (m, 4H, H_o), 3.46 (s, 4H, H_α), 3.02 (m, 1H, H_1), 1.08 (d, 6H, H_2, J = 6.6 Hz). ^{13}C NMR (75 MHz, CD_3CN) δ/ppm: 173.1 (C_β), 145.6 (C_i), 144.1 (C_p), 125.9 (C_m), 119.8 (C_o), 56.9 (C_α), 54.4 (C_1), 18.9 (C_2). ESI-MS (m/z): 831.2 (2M+H$^+$, 5%), 416.1 (M+H$^+$, 100%). MALDI-HRMS (m/z): calcd 416.1564 ($C_{19}H_{21}N_5O_6$ + H$^+$), found 416.1573. IR (KBr) $\tilde{\nu}$/cm^{-1}: 3349, 3180, 3137, 2969, 1688, 1598, 1545, 1511, 1362, 1174, 1080, 841, 752, 665, 495, 403. Ligand **L2** (41.5 mg) was heated in 5 mL of methanol and left to cool at room temperature. After 1 h, light green prismatic crystals suitable for X-ray single crystal analysis were obtained.

(*p*-Me$_2$N-Ph-imda)-*i*Pr, **L3**. Isopropylamine (80.8 µL, 0.9 mmol), ***p*-Me$_2$N-PhNH-COCH$_2$Cl**, **P3** (500.0 mg, 2.4 mmol), DIPEA (650.9 µL, 3.8 mmol), KI (156.1 mg, 0.9 mmol). Automated flash chromatography 0% → 1% methanol in dichloromethane, R_f = 0.35, 5% methanol in dichloromethane. Yield: 171.4 mg (0.42 mmol, 44%), white powder. ^{1}H NMR (300 MHz, CD_3CN) δ/ppm: 9.25 (s, 2H, H_N), 7.46-7.38 (m, 4H, H_o), 6.76-6.68 (m, 4H, H_m), 3.29 (s, 4H, H_α), 2.99 (m, 1H, H_1), 2.87 (s, 12H, $H_{N(CH_3)_2}$) 1.07 (d, 6H, H_2, J = 6.6 Hz). ^{13}C NMR (75 MHz, CD_3CN) δ/ppm: 171.0 (C_β), 148.8 (C_p), 129.5 (C_i), 122.2 (C_o), 113.8 (C_m), 56.5 (C_α), 54.0 (C_1), 41.1 ($C_{N(CH_3)_2}$), 18.8 (C_2). ESI-MS (m/z): 823.4 (2M+H$^+$, 6%), 412.2 (M+H$^+$, 100%). MALDI-HRMS (m/z): calcd 412.2707 ($C_{23}H_{33}N_5O_2$ + H$^+$), found 412.2694. IR (KBr) $\tilde{\nu}$/cm^{-1}: 3439, 3273, 3050, 2887, 2806, 1664, 1543, 1520, 1351, 1257, 818, 677, 522.

(Ph-imda)-Me, **L4**. Methylamine hydrochloride (63.7 mg, 0.9 mmol), **PhNH-COCH$_2$Cl, P1** (400.0 mg, 2.4 mmol), DIPEA (652.9 µL, 3.8 mmol), KI (156.6 mg, 0.9 mmol). Automated flash chromatography 0% → 10% methanol in dichloromethane, R_f = 0.32, 5% methanol in dichloromethane. Yield: 221.5 mg (0.74 mmol, 79%), white powder. ^{1}H NMR (300 MHz, CD_3CN) δ/ppm: 9.16 (s, 2H, H_N), 7.64 (d, 4H, H_o, J = 7.9 Hz) 7.34 (t, 4H, H_m, J = 7.9 Hz), 7.10 (t, 2H, H_p J = 7.4 Hz), 3.32 (s, 4H, H_α),2.48 (s, 3H, H_1). ^{13}C NMR (150 MHz, CD_3CN) δ/ppm: 170.0 (C_β), 139.5 (C_i), 129.8 (C_m), 124.8 (C_p), 120.7 (C_o), 62.4 (C_α), 43.8 (C_1). ESI-MS (m/z): 320.1 (M+Na$^+$, 21%), 298.1 (M+H$^+$, 59%). MALDI-HRMS (m/z): calcd 298.1550 ($C_{17}H_{19}N_3O_2$ + H$^+$), found 298.1560. IR (KBr) $\tilde{\nu}$/cm^{-1}: 3449, 3300, 3266, 2947, 1689, 1657, 1604, 1541, 1443, 1320, 1044, 854, 758, 692, 539, 507.

(Ph-imda)-Bn, **L5**. Benzylamine (128.8 µL, 1.2 mmol), **PhNH-COCH$_2$Cl, P1** (500.0 mg, 2.9 mmol), DIPEA (815.9 µL, 4.7 mmol), KI (195.7 mg, 1.2 mmol). Automated flash chromatography EtOAc:hexane gradient, R_f = 0.44 EtOAc:hexane = 8:2, R_f = 0.33, 3% methanol in dichloromethane. Yield: 284.6 mg (0.76 mmol, 65%), colorless oil. ^{1}H NMR (600 MHz, CD_3CN) δ/ppm: 9.29 (s, 2H, H_N), 7.60 (d, 4H, H_o, J = 8.2 Hz), 7.43 (d, 2H, H_{o1}, J = 7.8 Hz), 7.36-7.30 (m, 6H, H_m, H_{m1}), 7.25 (t, 1H, H_{p1}, J = 7.3 Hz), 7.09 (t, 2H, H_p, J = 7.4 Hz), 3.89 (s, 2H, H_1), 3.44 (s, 4H, H_α). ^{13}C NMR (75 MHz, CD_3CN) δ/ppm: 170.7, 139.5, 138.9, 130.3, 129.7, 129.4, 128.4, 124.7, 120.5, 60.3, 59.6. ESI-MS (m/z): 396.1 (M+Na$^+$, 12%), 374.1 (M+H$^+$, 100%). MALDI-HRMS (m/z): calcd 374.1863 ($C_{23}H_{23}N_3O_2$ + H$^+$), found 374.1887. IR (KBr) $\tilde{\nu}$/cm^{-1}: 3450, 3060, 3029, 1664, 1600, 1543, 1444, 1249, 1195, 754, 692, 504.

(Me$_2$N-Ph-imda)-Bn, **L6**. Benzylamine (109.2 µL, 0.9 mmol), ***p*-Me$_2$N-PhNH-COCH$_2$Cl, P3** (500.0 mg, 2.4 mmol), DIPEA (650.9 µL, 3.8 mmol), KI (156.1 mg, 0.9 mmol). Automated flash chromatography 0% → 10% methanol in dichloromethane, R_f = 0.37, 5% methanol in dichloromethane. Yield: 262.4 mg (0.57 mmol, 61%), white powder. ^{1}H NMR (300 MHz, CD_3CN) δ/ppm: 9.04 (s, 2H, H_N), 7.47-7.23 (m, 9H, H_{Ar}) 7.78-6.69 (m, 4H, H_{Ar}), 3.85 (s, 2H, H_1), 3.36 (s, 4H, H_α), 2.87 (s, 12H, $H_{N(CH_3)_2}$). ^{13}C NMR (75 MHz, CD_3CN) δ/ppm: 169.9, 148.9, 139.0, 130.2, 129.3, 129.2, 128.4, 122.3, 113.7, 60.3, 59.6, 41.0. ESI-MS (m/z): 460.2 (M+H$^+$, 100%). MALDI-HRMS (m/z): calcd 459.2634 ($C_{27}H_{33}N_5O_2$), found 459.2633. IR (KBr) $\tilde{\nu}$/cm^{-1}: 3445, 3261, 3061, 2883, 2800, 1657, 1600, 1521, 1320, 1256, 982, 817, 744, 700, 519.

Catalytic hydrogenation, general procedure. To a solution of **L5** or **L6** in methanol, palladium on carbon (10%) was added as a catalyst and the reaction in hydrogen atmosphere was performed overnight. The product was filtered and evaporated in a vacuum. The crude ligand was

purified by automated flash chromatography on a pre-packed silica gel column (12 g) yielding products in the form of white powder.

(Ph-imda)-H, **L7**. **L5** (459.6 mg, 1.23 mmol). Automated flash chromatography 0% → 10% methanol in dichloromethane, R_f = 0.25, 5% methanol in dichloromethane. Yield: 271.0 mg (0.96 mmol, 78%), white powder. ^{1}H NMR (300 MHz, CD_3CN) δ/ppm: 9.05 (s, 2H, H_N), 7.62 (d, 4H, H_o, J = 8.0 Hz), 7.33 (t, 4H, H_m, J = 7.9 Hz), 7.09 (t, 2H, H_p, J = 7.4 Hz), 3.42 (s, 4H, H_α). ^{13}C NMR (150 MHz, CD_3CN) δ/ppm: 171.0 (C_β), 139.5 (C_i), 129.7 (C_m), 124.7 (C_p), 120.5 (C_o), 53.9 (C_α). ESI-MS (m/z): 306.1 (M+Na$^+$, 28%), 284.1 (M+H$^+$, 100%). MALDI-HRMS (m/z): calcd 306.1213 ($C_{16}H_{17}N_3O_2$ + Na$^+$), found 306.1220. IR (KBr) $\tilde{\nu}$/cm^{-1}: 3373, 3281, 3056, 2877, 1656, 1599, 1530, 1442, 1300, 1151, 754, 692, 560, 485.

(*p*-Me$_2$N-Ph-imda)-H, **L8**. **L6** (260.0 mg, 0.57 mmol). Automated flash chromatography 0% → 5% methanol in dichloromethane (R_f = 0.16, 5% methanol in dichloromethane) Yield: 77.3 mg (0.21 mmol, 37%), white powder. ^{1}H NMR (600 MHz, CD_3CN) δ/ppm: 8.75 (s, 2H, H_N), 7.43-7.38 (m, 4H, H_o), 6.75-6.70 (m, 4H, H_m), 3.36 (s, 4H, H_α), 2.88 (s, 12H, $H_{N(CH_3)_2}$). ^{13}C NMR (75 MHz, CD_3CN) δ/ppm: 170.2 (C_β), 148.9 (C_p), 129.2 (C_i), 122.4 (C_o), 113.8 (C_m), 53.9 (C_α), 41.0 ($C_{N(CH_3)_2}$). ESI-MS (m/z): 739.3 (2M+H$^+$, 26%), 392.1 (M+Na$^+$, 13%), 370.1 (M+H$^+$, 100%). MALDI-HRMS (m/z): calcd 370.2237 ($C_{20}H_{27}N_5O_2$ + H$^+$), found 370.2260. IR (KBr) $\tilde{\nu}$/cm^{-1}: 3442, 3272, 2922, 2800, 1656, 1639, 1535, 1522, 1382, 1353, 948, 817, 602, 521.

Synthesis of metal complexes (ML_2), general procedure. Saturated methanol solutions of the ligand (2 eq) and metal salt (1 eq) were heated and boiled shortly in separate beakers until completely dissolved. The metal salt solution was added to the ligand solution and the mixture was cooled to room temperature and left partially covered for slow evaporation until crystals appeared (1 hour to 1 month). The solvent was decanted and the crystals washed with diethyl ether (2 x 2 mL) and air-dried. Complexes that did not crystallize by method of slow evaporation were placed in a tank with hexane or diethyl ether for slow diffusion.

[Zn(L1)$_2$](BF$_4$)$_2$ × 2CH$_3$OH, **1$_{Zn}$**. Ligand **L1** (64.7 mg, 0.2 mmol), $Zn(BF_4)_2 \times H_2O$ (23.8 mg, 0.1 mmol). The vial was partly covered and left in the fume hood for slow evaporation at room temperature for 1 week. Yield: 49.0 mg (0.05 mmol, 51%), colorless crystals, suitable for X-ray single crystal analysis. ^{1}H NMR (300 MHz, CD_3CN) δ/ppm: 9.34 (s, 4H, H_N), 7.48 (d, J = 8.0 Hz, 8H, H_o), 7.40 (t, J = 7.8 Hz, 8H, H_m), 7.25 (t, J = 7.3 Hz, 4H, H_p), 4.02 (d, J = 17.0 Hz, 4H, H_α), 3.65 (d, J = 16.8 Hz, 4H, H_α), 3.47 – 3.35 (m, 2H, H_i), 1.31 (d, J = 6.5 Hz, 12H, H_2). ^{13}C NMR (151 MHz, CD_3CN) δ/ppm: 173.0 (C_β), 136.8 (C_i), 130.2 (C_m), 127.3 (C_p), 122.1 (C_o), 57.8 (C_α), 56.8 (C_i), 18.4 (C_2). MALDI-HRMS (m/z): calcd for $C_{38}H_{45}N_6O_4Zn^+$ [M—2BF$_4^-$—H$^+$] 713.2783; found 713.2889. IR (KBr) $\tilde{\nu}$/cm^{-1}: 3640, 3542, 3336, 3104, 2981, 1644, 1598, 1567, 1500, 1452, 1327, 1082, 758, 692, 498, 448.

[Co(L1)$_2$](BF$_4$)$_2$ × 2CH$_3$OH, **1$_{Co}$**. Ligand **L1** (64.7 mg, 0.2 mmol), $Co(BF_4)_2 \times 6H_2O$ (33.7 mg, 0.1 mmol). The vial was partly covered and left in the fume hood for slow evaporation at room temperature for 1 day. Yield: 57.9 mg (0.06 mmol, 61%), pink crystals, suitable for X-ray single crystal analysis. MALDI-HRMS (m/z): calcd for $C_{38}H_{45}N_6O_4Co^+$ [M—2BF$_4^-$—H$^+$] 708.2823; found 708.2846. IR (KBr) $\tilde{\nu}$/cm^{-1}: 3534, 3362, 3068, 2972, 1637, 1598, 1568, 1452, 1327, 1053, 759, 692, 499, 454.

[Ni(L1)$_2$](BF$_4$)$_2$ × 2CH$_3$OH, **1$_{Ni}$**. Ligand **L1** (64.7 mg, 0.2 mmol), $Ni(NO_3)_2 \times 6H_2O$ (30.1 mg, 0.1 mmol), $NaBF_4$ (22.3 mg, 0.2 mmol). The vial was partly covered and left in the fume hood for slow evaporation at room temperature for 1 hour. Yield: 77.4 mg (0.08 mmol, 82%), blue-green crystals, suitable for X-ray single crystal analysis. MALDI-HRMS (m/z): calcd for $C_{38}H_{45}N_6O_4Ni^+$ [M–2BF$_4^-$–H$^+$] 707.2845; found 707.2867. IR (KBr) $\tilde{\nu}$/cm^{-1}: 3530, 3362, 3066, 2976, 1636, 1598, 1567, 1453, 1327, 1062, 692, 500, 458.

[Cu(L1)$_2$]$_2$(BF$_4$)$_2$(SiF$_6$) × 2H$_2$O, **1$_{Cu}$**. Ligand **L1** (21.5 mg, 0.07 mmol), $Cu(BF_4)_2 \times H_2O$ (7.84 mg, 0.03 mmol). The vial was partly covered and left in the fume hood for slow evaporation at room temperature for 4 days. Yield: 12.9 mg (0.01 mmol, 45%), pale green crystals, suitable for X-ray single crystal analysis. IR (KBr) $\tilde{\nu}$/cm^{-1}: 3444, 3288, 3211, 3099, 2978, 1668, 1621, 1596, 1566, 1384, 1345, 1125, 1083, 754, 693, 520.

[Zn(L3)$_2$](BF$_4$)$_2$, **3$_{Zn}$**. Ligand **L3** (18.3 mg, 0.04 mmol), $Zn(BF_4)_2 \times H_2O$ (5.3 mg, 0.02 mmol). The vial was partly covered and left in the fume hood for slow evaporation for 1 week then the vial was placed in a tank with diethyl ether (10 mL) for diffusion for 2 weeks. Yield: 14.2 mg (0.01 mmol, 61%), white solid. ^{1}H NMR (600 MHz, CD_3CN) δ/ppm: 9.26 (s, 4H), 7.33 (d, J = 8.6 Hz, 8H), 6.78 (d, J = 8.5 Hz, 8H), 3.96 (d, J = 16.5 Hz, 4H), 3.58 (d, J = 16.5 Hz, 4H), 3.42 – 3.27 (m, 2H), 2.92 (s, 24H), 1.29 (d, J = 6.2 Hz, 12H). ^{13}C NMR (151 MHz, CD_3CN) δ/ppm: 171.7, 149.2, 127.0, 123.2, 114.0, 57.4, 56.5, 41.2, 18.3. MALDI-HRMS (m/z): calcd for $C_{46}H_{65}N_{10}O_4Zn^+$ [M—2BF$_4^-$—H$^+$] 885.4471; found 885.4482. IR (KBr) $\tilde{\nu}$/cm^{-1}: 3318, 3082, 2980, 2889, 2807, 1633, 1522, 1325, 1083, 819, 520.

[Ni(L3)$_2$](BF$_4$)$_2$, **3$_{Ni}$**. Ligand **L3** (17.4 mg, 0.04 mmol), $Ni(NO_3)_2 \times 6H_2O$ (6.1 mg, 0.02 mmol), $NaBF_4$ (4.6 mg, 0.04 mmol). The vial was partly covered and left in the fume hood for slow evaporation for 1 day. Yield: 15.1 mg (0.02 mmol, 82%), light blue plate-like crystals suitable for X-ray single crystal analysis. MALDI-HRMS (m/z): calcd for $C_{46}H_{65}N_{10}NiO_4^+$ [M–2BF$_4^-$–H$^+$] 879.4533; found 879.4570. IR (KBr) $\tilde{\nu}$/cm^{-1}: 3441, 3060, 2975, 1626, 1521, 1384, 1083, 946, 818, 532, 523.

[Zn(L4)$_2$](BF$_4$)$_2$, **4$_{Zn}$**. Ligand **L4** (22.3 mg, 0.07 mmol), $Zn(BF_4)_2 \times H_2O$ (9.0 mg, 0.04 mmol). The vial was partly covered and left in the fume hood for slow evaporation at room temperature for 3 days. Yield: 25.1 mg (0.03 mmol, 80%), colorless plate-like crystals. ^{1}H NMR (300 MHz, CD_3CN) δ/ppm: 9.47 (s, 2H), 7.56 (d, J = 8.0 Hz, 4H), 7.39 (t, J = 7.9 Hz, 4H), 7.24 (t, J = 7.4 Hz, 2H), 3.94 (s, 4H), 2.64 (s, 3H). ^{13}C NMR (75 MHz, CD_3CN) δ/ppm: 171.8, 137.1, 130.2, 127.2, 121.9, 61.0, 45.0. MALDI-HRMS (m/z): calcd for $C_{34}H_{37}N_6O_4Zn^+$ [M–2BF$_4^-$–H$^+$] 657.2157; found 657.2151. IR

(KBr) $\tilde{\nu}$/cm^{-1}: 3335, 3158, 3103, 1635, 1598, 1566, 1499,1453, 1321, 1083, 757, 691, 504, 478.

[Ni(L4)$_2$](NO$_3$)$_2$, 4n$_{Ni}$. Ligand **L4** (59.5 mg, 0.2 mmol), Ni(NO$_3$)$_2$ × 6H$_2$O (30.1 mg, 0.1 mmol). The vial was partly covered and left in the fume hood for slow evaporation at room temperature for 1 day. Yield: 59.4 mg (0.07 mmol, 71%), blue crystals, suitable for X-ray single crystal analysis. MALDI-HRMS (m/z): calcd for $C_{34}H_{37}N_6O_4Ni^+$ [M–2BF$_4^-$–H$^+$] 651.2219; found 651.2229. IR (KBr) $\tilde{\nu}$/cm^{-1}: 3432, 3216, 3063, 2927, 1634, 1597, 1566, 1499, 1452, 1384, 1325, 1042, 964, 900, 767, 751, 690, 585, 499, 455, 429.

[Zn(L5)$_2$](BF$_4$)$_2$, 5$_{Zn}$. Ligand **L5** (19.0 mg, 0.05 mmol), Zn(BF$_4$)$_2$ × H$_2$O (6.1 mg, 0.02 mmol). The vial was partly covered and left in the fume hood for slow evaporation for 1 week then the vial was placed in a tank with diethyl ether (10 mL) for diffusion for 1 week. Yield: 15.1 mg (0.02 mmol, 60%), colorless plate-like crystals, ^{1}H NMR (300 MHz, CD$_3$CN) δ/ppm: 9.59 (s, 4H), 7.67 – 7.15 (m, 30H), 4.40 – 3.48 (m, 12H). ^{13}C NMR (75 MHz, CD$_3$CN) δ/ppm: 171.8, 137.1, 133.2, 130.2, 129.8, 127.2, 122.1, 58.3, 57.1. MALDI-HRMS (m/z): calcd for $C_{46}H_{45}N_6O_4Zn^+$ [M–2BF$_4^-$–H$^+$] 809.2783; found 809.2825. IR (KBr) $\tilde{\nu}$/cm^{-1}: 3442, 3068, 1632, 1566, 1082, 751, 706, 486.

[Ni(L5)$_2$](NO$_3$)$_2$, 5n$_{Ni}$. Ligand **L5** (16.2 mg, 0.04 mmol), Ni(NO$_3$)$_2$ × 6H$_2$O (6.32 mg, 0.02 mmol). The vial was partly covered and left in the fume hood for slow evaporation at room temperature for 10 days. Yield: 8.4 mg (0.01 mmol, 43%), light blue plate-like crystals, suitable for X-ray single crystal analysis. MALDI-HRMS (m/z): calcd for $C_{46}H_{45}N_6NiO_4^+$ [M–2BF$_4^-$–H$^+$] 803.2845; found 803.2845. IR (KBr) $\tilde{\nu}$/cm^{-1}: 3441, 3219, 3052, 1628, 1384, 1327, 761, 702.

[Zn(L6)$_2$](BF$_4$)$_2$, 6$_{Zn}$. Ligand **L6** (26.5 mg, 0.06 mmol), Zn(BF$_4$)$_2$ × H$_2$O (6.9 mg, 0.03 mmol). The vial was partly covered and left in the fume hood for slow evaporation for 1 week then the vial was placed in a tank with diethyl ether (10 mL) for diffusion for 1 week. Yield: 20.6 mg (0.02 mmol, 61%) colorless plate-like crystals, suitable for X-ray single crystal analysis. ^{1}H NMR (300 MHz, CD$_3$CN) δ/ppm: 9.37 (s, 4H), 7.46 (s, 10H), 7.39 (d, J = 9.1 Hz, 8H), 6.72 (d, J = 9.1 Hz, 8H), 4.01 (s, 4H), 3.97 – 3.43 (m, 8H), 2.89 (s, 24H). ^{13}C NMR (151 MHz, CD$_3$CN) δ/ppm: 170.4, 150.0, 133.2, 130.1, 129.7, 126.1, 123.3, 113.2, 58.0, 56.7, 40.6. MALDI-HRMS (m/z): calcd for $C_{54}H_{65}N_{10}O_4Zn^+$ [M–2BF$_4^-$–H$^+$] 981.4471; found 981.4503. IR (KBr) $\tilde{\nu}$/cm^{-1}: 3431, 2888, 1627, 1521, 1082, 816, 747, 703, 520.

[Zn(L7)$_2$](BF$_4$)$_2$, 7$_{Zn}$. Ligand **L7** (22.2 mg, 0.08 mmol), Zn(BF$_4$)$_2$ × H$_2$O (9.4mg, 0.04 mmol). The vial was placed in a tank with hexane (10 mL) for diffusion for 1 month. Yield: 21.5 mg (0.03 mmol, 71%) colorless crystals, suitable for X-ray single crystal analysis. ^{1}H NMR (300 MHz, CD$_3$CN) δ/ppm: 9.21 (s, 4H), 7.56 (d, J = 7.9 Hz, 8H), 7.37 (t, J = 7.8 Hz, 8H), 7.20 (t, J = 7.4 Hz, 4H), 3.80 (s, 8H). ^{13}C NMR (75 MHz, CD$_3$CN) δ/ppm: 172.9, 137.7, 130.1, 126.5, 121.5, 52.8. IR (KBr) $\tilde{\nu}$/cm^{-1}: 3443, 3344, 1641, 1564, 1084, 756, 691.

[Zn(L8)$_2$](BF$_4$)$_2$, 8$_{Zn}$. Ligand **L8** (12.85 mg, 0.04 mmol), Zn(BF$_4$)$_2$ × H$_2$O (4.2 mg, 0.02 mmol). The vial was partly covered and left in the fume hood for slow evaporation for 1 week then the vial was placed in a tank with diethyl ether (10 mL) for diffusion for 1 week. No crystallization occurred so the product was evaporated to dryness. Yield: 10.9 mg (0.01 mmol, 64%), light green solid. ^{1}H NMR (600 MHz, CD$_3$OD) δ/ppm: 7.40 (d, J = 9.0 Hz, 8H), 6.76 (d, J = 9.0 Hz, 8H), 3.58 (s, 8H), 2.90 (s, 24H). ^{13}C NMR (151 MHz, CD$_3$OD) δ/ppm: 171.6, 150.2, 127.8, 123.2, 114.0, 52.7, 41.0. MALDI-HRMS (m/z): calcd for $C_{40}H_{53}N_{10}O_4Zn^+$ [M–2BF$_4^-$–H$^+$] 801.3532; found 801.3640. IR (KBr) $\tilde{\nu}$/cm^{-1}: 3432, 2922, 1631, 1522, 1323, 1083, 818, 731, 522, 477.

***In situ* NMR measurements.** Complexes were prepared by dissolving the ligand and metal salt in different ratios in approximately 0.6 mL of deuterated solvent in an NMR tube. For preparing **ML$_2$** complexes, the ratio was 2L : 1M^{2+}, and for preparing **ML** complexes, the ratio was 1L : 4-6 M^{2+}.

NMR titrations. Ligand **L1** (5.4 mg) was dissolved in 2 mL CD$_3$CN (c(**L1**)= 8.3 mM) and Zn(BF$_4$)$_2$ × H$_2$O (20 mg) was dissolved in 1 mL of the **L1** solution (c(Zn^{2+})= 83.7 mM), (no dilution method.[47] The ligand solution (600 µL) was placed in an NMR tube and the spectrum of the free ligand was acquired. For each following measurement, an aliquot of the Zn^{2+} in **L1** solution was added until the ratio of Zn^{2+}:**L1** was 3:1.

Paramagnetic Co(II) NMR. NMR spectroscopy is mainly used for characterization of diamagnetic compounds. However, by adjusting the acquisition parameters, spectra of paramagnetic species can be recorded, giving valuable information about the structure of the sample. The observed shift in paramagnetic complexes is a sum of the hypothetical shift of the isostructural diamagnetic complex and the paramagnetic contribution which is further divided into the contact (scalar) and dipolar (pseudo-contact) shift (Equation 1).[48,49]

$$\delta_T^{exp} = \delta_T^{para} + \delta^{dia} = \delta_T^{con} + \delta_T^{dip} + \delta^{dia} \quad (1)$$

The contact shift, δ_T^{con}, describes the influence of the unpaired electron spin on nuclear chemical shifts due to through-bond hyperfine coupling. As the number of bonds between the examined nucleus and the paramagnetic metal ion increases, the value of the contact shift decreases and becomes negligible if the number of bonds between the paramagnetic metal ion and the nucleus is greater than four, and there are no π bonds. The dipolar shift, δ_T^{dip}, describes the through-space interaction of the magnetic moments of the unpaired electron and the nucleus and can be observed at distances up to 60 Å from the paramagnetic ion.

X-ray crystallography. The X-ray intensity data were collected on Oxford diffraction Xcalibur CCD diffractometer using monochromatic Cu-Kα (λ = 1.54184 Å) radiation. For temperature conditions see Table S1. The data were processed with CrysalisPro program[50] (unit cell determination and data reduction). Due to absence of several symmetry independent reflections at higher angles, the data up to Θ_{max} = 65° were taken into calculations for crystals of **1$_{Zn}$**, **1$_{Co}$**, **1$_{Ni}$** and **5n$_{Ni}$**. The crystal of **7$_{Zn}$** diffracted up to Θ_{max} = 62°. The structures were solved by direct methods with SIR2011 program[51] and refined against F^2 on all data by a

full-matrix least squares procedure with SHELXL-97 program.[52] The exception was the structure of **6**$_{Zn}$, where each least square cycle was separated into 5 sub-cycles (BLOC instruction), due to large number of parameters in the structure (3 symmetrically nonequivalent **[Zn(L6)$_2$]**$^{2+}$ complex cations and 6 symmetrically nonequivalent BF_4^- anions). In 1st sub-cycle only the position and displacement parameters for residue 1 were refined (1st **[Zn(L6)$_2$]**$^{2+}$ complex), in 2nd (3rd) sub-cycles similar parameters for residues 2 (3) were refined (2nd and 3rd **[Zn(L6)$_2$]**$^{2+}$ complexes, respectively), in 4th sub-cycle position and displacement parameters for BF_4^- anions were refined (residues 4, 5, 6, 7, 8 and 9) and in last 5th sub-cycle only position parameters for all atoms were refined. These 5 sub-cycles were repeated until overall convergence of all parameters in structure was reached. All non-hydrogen atoms in all structures were refined anisotropically and rigid group restraints (DELU) were applied only for atoms in structure of **6**$_{Zn}$, due to large number of parameters. Also, in the structure of **6**$_{Zn}$, BF_4^- anions were treated as rigid bodies of ideal tetrahedral symmetry with B—F bond length of 1.36 Å. Additionally, in the structure of **6**$_{Zn}$, the two solvent accessible voids of volume 600 Å^3 (forming infinite cylindrical shapes) contained unresolved solvent contribution. Electron density from this voids were treated by SQUEEZE option in PLATON program[53,54] and contribution of 202 electrons per void (as found by SQUEEZE calculation) were removed from the observed intensities. Final refinement of the rest part of the structure (3 **[Zn(L6)$_2$]**$^{2+}$ complexes and 6 BF_4^- anions) was performed without contribution from these voids.

During refinement of structure **7**$_{Zn}$, orientational disorder of one phenyl ring (with attached N—H group) from one of the ligands coordinated to Zn atom was observed. The electron density was modeled as two identical parts and occupation parameter for each part was refined, with constraint that sum of occupations is 1. The phenyl rings in these parts were treated as perfect hexagons with C—C bond lengths of 1.39 Å. C—N bond lengths which included disordered N atoms was restrained to be equal to other chemically identical bond lengths in molecule (SADI restraint), while displacement parameters were restrained to behave isotropically (ISOR restraint). Amide hydrogen atoms on all compounds were refined freely and isotropically, the exceptions were structures of **6**$_{Zn}$ and **7**$_{Zn}$, where they have been calculated from position parameters of atoms on which they are bonded assuming ideal sp^2 hybridization, N—H bond length of 0.86 Å and U(H)= 1.2×U$_{eq}$(N) (HFIX 43). Secondary amine hydrogen atoms bonded to coordinated nitrogen atoms in structure **7**$_{Zn}$ were also calculated, assuming ideal sp^3 hybridization, N—H bond length of 0.91 Å and U(H)= 1.2×U$_{eq}$(N) (HFIX 13).

All hydrogen atoms bonded to carbon atoms were included in the structural model at geometrically calculated positions. For methyl hydrogen atoms the torsional angles around C—C (N—C) bonds were refined (HFIX 137), except in structure **6**$_{Zn}$, where the staggered conformation with respect to second N—C(Phe) bond was used (HFIX 33). Hydroxyl hydrogen atoms on several methanol solvent molecules were constrained to ideal distance of 0.96 Å and C–O–H angle of 109°, while their torsions with respect to C–O bond were refined (HFIX 147). Additional distance restraints with nearest possible acceptor atoms were used. During refinement it was observed that anisotropic displacement parameters in BF_4^- anions were unusually large, especially in structure **6**$_{Zn}$. Such disorder is very often in structures containing these anions.[55] Their occupancies were not refined (they are constrained to 1), because this would violate the charge neutrality of the structures. All details for X-ray diffraction studies in this publication are collected in Table 3. The CCDC 1938663-1938672 refcodes contain the supplementary crystallographic data for this paper. These data can be obtained free of charge from The Cambridge Crystallographic Data Centre via www.ccdc.cam.ac.uk/data_request/cif.

Computational details. All molecular geometries were optimized using a very efficient DFT M05-2X/6-31+G(d)/LanL2DZ + ECP model, known to be successful in reproducing geometries, dipole moments and hemolytic bond energies in various zinc complexes.[56,57] To account for the effect of the acetonitrile solution, during geometry optimization we included the implicit SMD solvation model (ε = 35.688), being in line with our earlier results.[15] Thermal corrections were extracted from the corresponding frequency calculations, and all of the presented results correspond to differences in the Gibbs free energies. All calculations were performed using the Gaussian 16 software.[58] Cartesian coordinates for all computed molecules are collected in a single text file readable by the program Mercury (version 3.3 or later).[59]

Analysis of the coordination geometry. The first method A[37] employs two structural parameters, see Scheme 2: the twist angle ϕ between two triangles and the s/h ratio (s-length of the triangle side, h-distance between two triangles). Ideal values for ϕ are 60° (regular octahedron) and 0° (trigonal prism), and an ideal value of the s/h ratio in the case of regular octahedron is 1.22. The trigonal prism has a compression ratio *(s/h)* uniformly close to 1.00 (range 0.96-1.04).[37]

The second method B[38] defines three geometrical parameters, see Scheme 3: the θ-angle between the triangle plane (basis) and plane defined by one atom in the triangle plane, metal ion and atom in the lower triangle plane regarded as

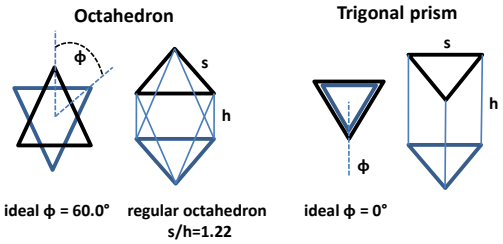

Scheme 2. Method A for classification of hexacoordinated polyhedra with two parameters-ϕ and s/h ratio.[37]

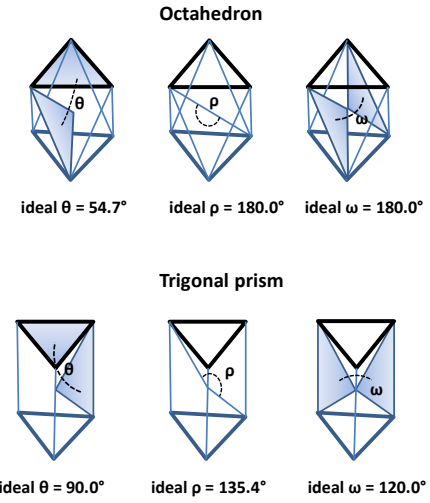

Scheme 3. Method B for classification of hexacoordinated polyhedra with three parameters-θ,ρ and ω.[38]

"analogous" to the atom in the above triangle plane, ρ-angle between two "bonds" of "trans" atoms in two triangle planes to the metal ion while the third parameter ω is defined depending whether the polyhedron in question is regarded as an octahedron or trigonal prism. If the polyhedron is regarded as an octahedron, then ω is the angle between two opposite planes. If it is regarded as a trigonal prism, then ω is an angle between neighboring planes. Therefore, in this scheme it this necessary to assume type of the polyhedron before calculating the ω parameter making the scheme somewhat arbitrary. In the part of calculations according to the first two methods, SymPy library was employed[60] and the parameters shown in Tables S7 and S8 (with the exception of parameter h in method A) are average values of the calculated parameters.

The third method C[39] presents a generalization with respect to the former two schemes[37,38] since it treats different coordination numbers (from two to nine) and the set of corresponding polyhedra. On the contrary, methods A and B take into account only two possible hexacoordinated polyhedra: octahedron and trigonal prism. In addition, in methods A and B the orientation of the polyhedron (choice of the triangle bases) is not unique providing additional imprecision in the subsequent analysis. Method C is implemented in the program FindGeo[40] which is available as a standalone or web application. The FindGeo program compares polyhedra around metal ion with templates from a library and determines the best match, e. q. the lowest root mean square deviation (RMSD) for different atom-atom pairings between the analyzed polyhedron and each template from the library.[39] It should be noted that the algorithm even takes into account possibility of ligand atom vacancy around the analyzed polyhedron.

ASSOCIATED CONTENT

Supporting Information

Spectroscopic characterization of ligands and complexes (NMR, ESI MS, IR), Cartesian coordinates for all computed molecules in a single separate text file, crystallographic data in cif format. CCDC 1938663-1938672. For ESI see DOI: The Supporting Information is available free of charge on the ACS Publications website.

AUTHOR INFORMATION

Corresponding Author

*E-mail: Srecko.Kirin@irb.hr

ORCID

Natalija Pantalon Juraj: 0000-0002-0357-5817
Berislav Perić: 0000-0002-2397-2836
Robert Vianello: 0000-0003-1779-4524
Srećko I. Kirin: 0000-0002-0500-2422

ACKNOWLEDGMENT

These materials are based on work financed by the Croatian Science Foundation (HrZZ, project numbers IP-2014-09-1461 and IP-2014-09-3386). The authors thank Ernest Sanders (Ruđer Bošković Institute) for technical assistance.

REFERENCES

(1) Hart, J. R. Ethylenediaminetetraacetic Acid and Related Chelating Agents. *Ullmann's Encyclopedia of Industrial Chemistry*, 2000.

(2) Oviedo, C.; Rodríguez, J. EDTA: The Chelating Agent under Environmental Scrutiny. *Quím. Nova*. **2003**, 26 (6), 901–905.

(3) Skoog, D. A.; Holler, F. J.; Crouch, S. R.; West, D. M. *Skoog and West's Fundamentals of Analytical Chemistry*; Belmont: Brooks/Cole, **2014**.

(4) Fernández, R. G.; García Alonso, J. I. Separation of Rare Earth Elements by Anion-Exchange Chromatography Using Ethylenediaminetetraacetic Acid as Mobile Phase. *J. Chromatogr. A*. **2008**, *1180* (1), 59–65.

(5) Whittaker, P.; Vanderveen, J. E.; Dinovi, M. J.; Kuznesof, P. M.; Dunkel, V. C. Toxicological Profile, Current Use, and Regulatory Issues on EDTA Compounds for Assessing Use of Sodium Iron EDTA for Food Fortification. *Regul. Toxicol. Pharmacol.* **1993**, *18* (3), 419–427.

(6) Hochuli, E.; Döbeli, H.; Schacher, A. New Metal Chelate Adsorbent Selective for Proteins and Peptides Containing Neighbouring Histidine Residues. *J. Chromatogr. A* **1987**, *411*, 177–184.

(7) Rousseau, J.; Zhang, Z.; Dias, G. M.; Zhang, C.; Colpo, N.; Bénard, F.; Lin, K.-S. Design, Synthesis and Evaluation of Novel Bifunctional Tetrahydroxamate Chelators for PET Imaging of ^{89}Zr-Labeled Antibodies. *Bioorg. Med. Chem. Lett.* **2017**, *27* (4), 708–712.

(8) Rousseau, J.; Zhang, Z.; Wang, X.; Zhang, C.; Lau, J.; Rousseau, E.; Čolović, M.; Hundal-Jabal, N.; Bénard, F.; Lin, K.-S. Synthesis and Evaluation of Bifunctional Tetrahydroxamate Chelators for Labeling Antibodies with ^{89}Zr for Imaging with Positron Emission Tomography. *Bioorg. Med. Chem. Lett.* **2018**, *28* (5), 899–905.

(9) Fryxell, G. E.; Chouyyok, W.; Rutledge, R. D. Design and Synthesis of Chelating Diamide Sorbents for the Separation of Lanthanides. *Inorg. Chem. Commun.* **2011**, *14* (6), 971–974.

(10) Bulbul Sonmez, H.; Senkal, B.; Bicak, N. Polymer-supported Iminodiacetamides for Selective Mercury Extraction. *J. Appl. Polym. Sci.* **2003**, 87, 1316–1321.

(11) Urbanova, N.; Kadar, M.; Toth, K.; Bogati, B.; Andruch, V.;

Bitter, I.; Urbanová, N.; Kádár, M.; Tóth, K.; Bogáti, B. Fluorescent Iminodiacetamide Derivatives as Potential Ionophores for Optical Zinc Ion-Selective Sensors. *Anal. Sci.* **2008**, *24* (6), 727–733.

(12) Smrečki, N.; Rončević, T.; Jović, O.; Kukovec, B.-M.; Maravić, A.; Gajski, G.; Čikeš-Čulić, V. Copper(II) Complexes with N′ -Methylsarcosinamide Selective for Human Bladder Cancer Cells. *Inorganica Chim. Acta* **2019**, *488*, 312–320.

(13) Heering, C.; Francis, B.; Nateghi, B.; Makhloufi, G.; Lüdeke, S.; Janiak, C. Syntheses, Structures and Properties of Group 12 Element (Zn, Cd, Hg) Coordination Polymers with a Mixed-Functional Phosphonate-Biphenyl-Carboxylate Linker. *CrystEngComm* **2016**, *18* (27), 5209–5223.

(14) Cremades, E.; Echeverría, J.; Alvarez, S. The Trigonal Prism in Coordination Chemistry. *Chem. Eur. J.* **2010**, *16* (34), 10380–10396.

(15) Škalamera, Đ.; Sanders, E.; Vianello, R.; Maršavelski, A.; Pevec, A.; Turel, I.; Kirin, S. I. Synthesis and Characterization of ML and ML_2 Metal Complexes with Amino Acid Substituted Bis(2-Picolyl)Amine Ligands. *Dalton Trans.* **2016**, *45* (7), 2845–2858.

(16) Smrečki, N.; Kukovec, B. M.; Đaković, M.; Popović, Z. A Diversity of Hydrogen Bond Motifs in the Crystal Structures of Nickel(II) and Copper(II) Complexes with N-Arylalkyliminodiacetamides. *Polyhedron* **2015**, *93*, 106–117.

(17) Smrečki, N.; Jović, O.; Molčanov, K.; Kukovec, B.-M.; Kekez, I.; Matković-Čalogović, D.; Popović, Z. Influence of the Non-Coordinating Alkyl Chain Type in N-Alkylated Iminodiacetamides on the Stability and Structure of Their Complexes with Nickel(II) and Cobalt(II). *Polyhedron* **2017**, *130*, 115–126.

(18) Sekizaki, M. Bis(Iminodiacetamide)Nickel(II) Perchlorate. *Acta Cryst.* **1976**, *B32*, 1568–1570.

(19) Müller, E.; Bayer, O.; Meerwein, H.; Ziegler, K. Band XI/2 – Stickstoffverbindungen II und III. In *Methoden der Organischen Chemie (Houben Weyl), Band XI/2 – Stickstoffverbindungen II und III*; Georg Thieme Verlag: Stuttgart, 1958.

(20) Wen, Y.; Chen, X.; Wen, H.; Tang, X. Efficient Synthesis of Piperazinediones Using Potassium Iodide Catalysis in Aqueous Media. *Lett. Org. Chem.* **2011**, No. 8, 732–736.

(21) Diaz-Torres, R.; Alvarez, S. Coordinating Ability of Anions and Solvents towards Transition Metals and Lanthanides. *Dalton Trans.* **2011**, *40* (40), 10742–10750.

(22) Riddlestone, I. M.; Kraft, A.; Schaefer, J.; Krossing, I. Taming the Cationic Beast: Novel Developments in the Synthesis and Application of Weakly Coordinating Anions. *Angew. Chem. Int. Ed. Engl.* **2018**, *57* (43), 13982–14024.

(23) Rajput, L.; Sanphui, P.; Biradha, K. Effect of Substituents on Molecular Geometry and Self-Aggregation *Cryst. Growth Des.* **2007**, *7* (9), 1872–1880.

(24) Juraj, N. P.; Pennec, J. Le; Perić, B.; Kirin, S. I. A Case Study of Supramolecular Organization : One Ferrocene Substituted Iminodiacetamide and Its Chloroform Solvate. *Croat. Chem. Acta* **2018**, *90* (4), 613–623.

(25) Saihara, K.; Yoshimura, Y.; Fujimoto, H.; Shimizu, A. Detrimental Effect of Glass Sample Tubes on Investigations of BF_4^--Based Room Temperature Ionic Liquid–Water Mixtures. *J. Mol. Liq.* **2016**, *219*, 493–496.

(26) Casellas, H.; Pevec, A.; Kozlevčar, B.; Gamez, P.; Reedijk, J. An Unprecedented M_4-SiF_6^{2-}- Bridged Supramolecular Polymer Consisting of Bis-μ-F-Bridged Dinuclear Cu(II) Dications. *Polyhedron* **2005**, *24* (12), 1549–1554.

(27) Spek, A. Structure Validation in Chemical Crystallography. *Acta Crystallogr. Sect. D* **2009**, *65* (2), 148–155.

(28) Simmons, J. T.; Yuan, Z.; Daykin, K. L.; Nguyen, B. T.; Clark, R. J.; Shatruk, M.; Zhu, L. Bis[*N* -Alkyl- *N N* -Di(2-Pyridylmethyl)Amine]Zinc(II) Perchlorates Display *Cis-Facial* Stereochemistry in Solid State and Solution. *Supramol. Chem.* **2014**, *26* (3–4), 214–222.

(29) Bain, A. D.; Duns, G. J. Chemical Exchange Measurements in NMR. In *Analytical Spectroscopy Library*. **1997**, 227–263.

(30) Simmons, J. T.; Allen, J. R.; Morris, D. R.; Clark, R. J.; Levenson, C. W.; Davidson, M. W.; Zhu, L. Integrated and Passive 1,2,3-Triazolyl Groups in Fluorescent Indicators for Zinc(II) Ions: Thermodynamic and Kinetic Evaluations. *Inorg. Chem.* **2013**, *52* (10), 5838–5850.

(31) Marat, K. *SpinWorks 4 Software, University of Manitoba, Available from: https://home.cc.umanitoba.ca/~wolowiec/spinworks/index.html*.

(32) Sandstöm, J. *Dynamic NMR Spectroscopy*; Academic Press, 1982.

(33) Zimmer, K. D.; Shoemaker, R.; Ruminski, R. R. Synthesis and Characterization of a Fluxional Re(I) Carbonyl Complex *fac*-$[Re(CO)_3(Dpop')Cl]$ with the Nominally Tri-Dentate Ligand dipyrido(2,3-a:3′,2′-j)phenazine (dpop′). *Inorganica Chim. Acta* **2006**, *359* (5), 1478–1484.

(34) Dawson, D. M.; Ke, Z.; Mack, F. M.; Doyle, R. A.; Bignami, G. P. M.; Smellie, I. A.; Bühl, M.; Ashbrook, S. E. Calculation and Experimental Measurement of Paramagnetic NMR Parameters of Phenolic Oximate Cu(Ii) Complexes. *Chem. Commun.* **2017**, *53* (76), 10512–10515.

(35) Kruck, M.; Sauer, D. C.; Enders, M.; Wadepohl, H.; Gade, L. H. Bis(2-Pyridylimino)Isoindolato Iron(II) and Cobalt(II) Complexes: Structural Chemistry and Paramagnetic NMR Spectroscopy. *Dalton Trans.* **2011**, *40* (40), 10406–10415.

(36) Hansch, C.; Leo, A.; Taft, R. W. A Survey of Hammett Substituent Constants and Resonance and Field Parameters. *Chem. Rev.* **1991**, *91* (2), 165–195.

(37) Stiefel, E. I.; Brown, G. F. Detailed Nature of the Six-Coordinate Polyhedra in Tris(Bidentate Ligand) Complexes. *Inorg. Chem.* **1972**, *11* (2), 434–436.

(38) Banerjee, S.; Ghosh, A.; Wu, B.; Lassahn, P.-G.; Janiak, C. Polymethylene Spacer Regulated Structural Divergence in Cadmium Complexes: Unusual Trigonal Prismatic and Severely Distorted Octahedral Coordination. *Polyhedron* **2005**, *24* (5), 593–599.

(39) Andreini, C.; Cavallaro, G.; Lorenzini, S. FindGeo: A Tool for Determining Metal Coordination Geometry. *Bioinformatics* **2012**, *28* (12), 1658–1660.

(40) Tools: Tools @ MetalWeb, http://metalweb.cerm.unifi.it/tools/findgeo/

(41) Kokan, Z.; Perić, B.; Vazdar, M.; Marinić, Ž.; Vikić-Topić, D.; Meštrović, E.; Kirin, S. I. Metal-induced supramolecular chirality inversion of small self-assembled molecules in solution. *Chem. Commun.* **2017**, *53* (12), 1945–1948.

(42) Kokan, Z.; Kovačević, B.; Štefanić, Z.; Tzvetkova, P.; Kirin, S. I. Controlling orthogonal self-assembly through cis-trans isomerization of a non-covalent palladium complex dimer. *Chem. Commun.* **2018**, *54* (17), 2094–2097.

(43) Opačak, S.; Kokan, Z.; Glasovac, Z.; Perić, B.; Kirin, S. I. "Backdoor induction" of chirality: Trans-1,2-cyclohexanediamine as key building block for asymmetric hydrogenation catalysts. *Eur. J. Org. Chem.* **2019**, (11), 2115–2128.

(44) Pernar, M.; Kokan, Z.; Kralj, J.; Glasovac, Z.; Tumir, L.-M.; Piantanida, I.; Eljuga, D.; Turel, I.; Brozovic, A.; Kirin, S. I. Organometallic ruthenium(II)-arene complexes with triphenylphosphine amino acid bioconjugates: Synthesis, characterization and biological properties. *Bioorg. Chem.* **2019**, *87*, 432–446.

(45) Crans, D. C.; Yang, L.; Gaidamauskas, E.; Khan, R.; Jin, W.; Simonis, U. Applications of Paramagnetic NMR Spectroscopy for Monitoring Transition Metal Complex Stoichiometry and Speciation, *Paramagnetic Resonance of Metallobiomolecules*; ACS Symposium Series; American Chemical Society, **2003**, *858*, 17–304.

(46) Yang, L.; Crans, D. C.; Miller, S. M.; la Cour, A.; Anderson, O. P.; Kaszynski, P. M.; Godzala, M. E. 3rd; Austin, L. D.; Willsky, G. R. Cobalt(II) and Cobalt(III) Dipicolinate Complexes: Solid State, Solution, and in Vivo Insulin-like

Properties. *Inorg. Chem.* **2002**, *41* (19), 4859–4871.
(47) Thordarson, P. Determining Association Constants from Titration Experiments in Supramolecular Chemistry. *Chem. Soc. Rev.* **2011**, *40* (3), 1305–1323.
(48) Bren, K. L. Nuclear Magnetic Resonance (NMR) Spectroscopy of Metallobiomolecules. In *Encyclopedia of Inorganic Chemistry*; 2008.
(49) Pavlov, A. A.; Belov, A. S.; Savkina, S. A.; Polezhaev, A. V; Aleshin, D. Y.; Novikov, V. V; Nelyubina, Y. V. Synthesis and Spin State of the Cobalt(II) Complexes with Substituted 2,6-Bis(Pyrazol-3-yl)Pyridine Ligands. *Russ. J. Coord. Chem.* **2018**, *44* (8), 489–495.
(50) CrysAlisPro, Version 1.171.37.35, Rigaku OD, 2014.
(51) Burla, M. C.; Caliandro, R.; Camalli, M.; Carrozzini, B.; Cascarano, G. L.; Giacovazzo, C.; Mallamo, M.; Mazzone, A.; Polidori, G.; Spagna, R. SIR2011: A New Package for Crystal Structure Determination and Refinement. *J. Appl. Crystallogr.* **2012**, *45* (2), 357–361.
(52) Sheldrick, G. M. A Short History of SHELX. *Acta Crystallogr. A.* **2008**, *64* (Pt 1), 112–122.
(53) Spek, A. Single-Crystal Structure Validation with the Program PLATON. *J. Appl. Crystallogr.* **2003**, *36* (1), 7–13.
(54) van der Sluis, P.; Spek, A. L. BYPASS: An Effective Method for the Refinement of Crystal Structures Containing Disordered Solvent Regions. *Acta Crystallogr. Sect. A* **1990**, *46* (3), 194–201.
(55) J. J. Allen, A. R. Barron, http://cnx.org/content/M36687/1.3/ (from P. M. V. Raja and A. R. Barron, Physical Methods in Chemistry and Nano Science, Rice University).
(56) Amin, E. A.; Truhlar, D. G. Zn Coordination Chemistry: Development of Benchmark Suites for Geometries, Dipole Moments, and Bond Dissociation Energies and Their Use To Test and Validate Density Functionals and Molecular Orbital Theory. *J. Chem. Theory Comput.* **2008**, *4* (1), 75–85.
(57) Cramer, C. J.; Truhlar, D. G. Density Functional Theory for Transition Metals and Transition Metal Chemistry. *Phys. Chem. Chem. Phys.* **2009**, *11* (46), 10757–10816.
(58) Gaussian 16, Revision A.03, M. J. Frisch, G. W. Trucks, H. B. Schlegel, G. E. Scuseria, M. A. Robb, J. R. Cheeseman, G. Scalmani, V. Barone, G. A. Petersson, H. Nakatsuji, X. Li, M. Caricato, A. V. Marenich, J. Bloino, B. G. Janesko, R. Gomperts, B. Mennu.
(59) The program Mercury is available at no cost from www.ccdc.cam.ac.uk/products/mercury.
(60) Meurer A, Smith C. P.; Paprocki M.; Čertík O.; Kirpichev S. B.; Rocklin M.; Kumar A.; Ivanov S.; Moore J. K.; Singh S.; Rathnayake T.; Vig S.; Granger B. E.; Muller R. P.; Bonazzi F.; Gupta H.; Vats S.; Johansson F.; Pedregosa F.; Curry M. J.; Terrel A. R.; Roučka Š.; Saboo A.; Fernando I.; Kulal S.; Cimrman R.; Scopatz A. SymPy: Symbolic Computing in Python. *PeerJ Comput. Sci.* **2017**, *3:e103*.

Table of Contents artwork.